Polyelectrolyte Complex-Covalent Interpenetrating Polymer Network Hydrogels

Defu Li, Tobias Göckler, Ute Schepers, Samanvaya Srivastava

Defu Li, Tobias Göckler, Samanvaya Srivastava
Department of Chemical and Biomolecular Engineering, University of California, Los Angeles, Los Angeles, CA 90095, USA
Email: samsri@ucla.edu

Tobias Göckler, Ute Schepers
Institute of Functional Interfaces, Karlsruhe Institute of Technology, Hermann-von-Helmholtz-Platz 1, 76344 Eggenstein-Leopoldshafen, Germany

Samanvaya Srivastava
California NanoSystems Institute, University of California, Los Angeles, Los Angeles, CA 90095, USA
Center for Biological Physics, University of California, Los Angeles, Los Angeles, CA 90095, USA
Institute for Carbon Management, University of California, Los Angeles, Los Angeles, CA 90095, USA

Keywords: interpenetrating polymer network hydrogels, electrostatic self-assembly, polyelectrolyte complexation, block copolymers, polyelectrolytes

Polyelectrolyte complex (PEC) hydrogels possess a rich microstructural diversity and tunability of shear response, self-healing attributes, and pH- and salt-responsiveness. Yet, their utility in biotechnology and biomedicine has been limited, owing to their weak mechanical strength and uncontrolled swelling. Here, we introduce a strategy to overcome these drawbacks of PEC hydrogels by interlacing the electrostatically crosslinked PEC network with a covalently crosslinked polymer network, creating polyelectrolyte complex-covalent interpenetrating polymer network (PEC-IPN) hydrogels. In the PEC-IPN hydrogels demonstrated here, composed of oppositely charged ABA triblock copolymers and photocrosslinkable 4-arm poly(ethylene oxide) (PEO), the PEC network self-assembles

swiftly in aqueous environs, providing structural rigidity and serving as protective scaffoldings for the covalently crosslinkable PEO precursors. Photocrosslinking of the PEO chains creates a covalent network, supplying structural reinforcement to the PEC network. The resulting PEC-IPN hydrogels possess significantly improved shear and tensile strength, swelling characteristics, and mechanical stability in saline environments while preserving the intrinsic features of PEC networks, including the mesoscale network structure and salt-responsiveness. We envision that our approach to produce PEC based IPN hydrogels will pave the way for creation of self-assembled hybrid materials that harness the unique attributes of electrostatic self-assembly pathways, with broad applications in biomedicine.

1. Introduction

Polyelectrolyte complex (PEC) hydrogels[1-12] present an exciting platform for development of soft materials to cater to diverse applications in biomedicine[13, 14] as scaffolds for tissue engineering,[15-18] bioadhesives,[19-26] and drug delivery,[27-31] as well as ionic conductors[32, 33] and in food industries.[34, 35] These hydrogels self-assemble rapidly[1, 9] upon mixing of oppositely charged block polyelectrolytes and exhibit hierarchical microstructures,[4, 5, 36-39] comprising three-dimensional networks of PEC domains (composed of the oppositely charged blocks) connected to each other via the neutral blocks. This microstructure differentiates PEC hydrogels from ionically crosslinked hydrogels[40-47] (typically composed of homopolyelectrolytes) and contribute to their unique combination of attributes, including tunable shear properties,[2, 4-6, 9, 12, 48] stimuli (salt- and pH-) responsiveness,[1, 2, 4, 8, 9, 48] injectability,[12, 49] self-healing properties,[12, 49] and the ability to encapsulate charged macromolecules such as proteins and nucleic acids.[50-54]

Yet, broad applications of PEC hydrogels remain limited owing to their physical crosslinked structure contributing to low shear strength (typically less than 20 kPa), miniscule tensile strength, and an inherent coupling between the network microstructure and its shear response.[5] In contrast, applications such as tissue adhesion typically require hydrogel sealants to mimic shear properties of the tissue substrates (e.g., ~1 kPa for soft tissue, ~10 kPa for muscle, ~50 kPa for skin, > 100 kPa for cartilage and bone).[55-57] At the same time, PEC hydrogels swell indefinitely and eventually dissolve upon exposure to aqueous media, indicating degradation of hydrogel structure.[3, 58] Limited and tunable swelling can avoid material loss, preserve stability of structure and mechanical properties, and maintain the

functions of PEC hydrogels which can broaden their utility. However, effective measures for controlling swelling of PEC hydrogels remain elusive.

Here, we introduce a strategy to address these shortcomings of PEC hydrogels while retaining their unique attributes by interlacing the PEC network with a covalent network. Interpenetration of polymer networks has been employed to imbue properties like toughness and stimuli-responsiveness in hydrogels.[59-64] In this work, we demonstrate synergic improvements in the material properties of PEC-covalent interpenetrating polymer network (IPN) hydrogels which are not accessible in hydrogels composed of either of the two networks, including substantial improvements in mechanical strength, toughness, and swelling performance while conserving the microstructure of the PEC network. Moreover, our approach offers a strategy to expand the utility of photocrosslinkable hydrogels by enabling *in situ* crosslinking of the photocrosslinkable precursor polymers. The self-assembled PEC hydrogels provide a protective environment for the photocrosslinkable precursors, mitigating dilution and deactivation prior to their crosslinking. We envision that the PEC-covalent IPN platform demonstrated here will constitute the first steps towards implementation of PEC-based IPN hydrogels in future biomedical applications.

2. Results and Discussion

2.1. Self-Assembled PEC Networks as Protective Scaffoldings for Covalent Crosslinkable Polymers

PEC hydrogels self-assemble swiftly[65-68] upon mixing of aqueous solutions of oppositely charged block polyelectrolytes (bPEs) based on poly(ally glycidyl ether)$_{98}$-poly(ethylene oxide)$_{455}$-poly(ally glycidyl ether)$_{98}$ (PAGE-PEO-PAGE). The PAGE blocks were functionalized with ionic (guanidinium and sulfonate) moieties[1] (**Figure 1A**, row 1). These hydrogels are injectable and remain insoluble in water, even upon shaking, over a few minutes (**Figure 1B**, row 1, see also **Supplementary Movie SM1**).

Introduction of hydrophilic chemically crosslinkable 4-arm poly(ethylene oxide)$_{455}$ acrylate (PEO) did not impede with the PEC gel formation, resulting in injectable PEC+PEO hydrogels (**Figure 1A**, row 3). The electrostatically self-assembled PEC networks provide structural stability and insolubility in aqueous environments to the PEC+PEO hydrogels (**Figure 1B**, row 3, see also **Supplementary Movie SM2**). Moreover, the PEC networks serve as scaffoldings to protect the PEO precursors against uncontrolled dilution (**Figure 1B**, row 3). Ultraviolet (UV) irradiation of the PEC+PEO hydrogels for 5 minutes resulted in the formation of polyelectrolyte complex-interpenetrating polymer networks (PEC-IPN)

hydrogels composed of water-laden interlaced PEC and chemically crosslinked PEO networks (**Figure 1A**, row 3). In stark contrast, exposure of the solution of crosslinkable polymer precursors to aqueous environments prior to UV-induced crosslinking resulted in rapid dilution of the precursors, limiting their ability to form chemically crosslinked hydrogels (**Figures 1A and 1B**, row 2, see also **Supplementary Movie SM3**).

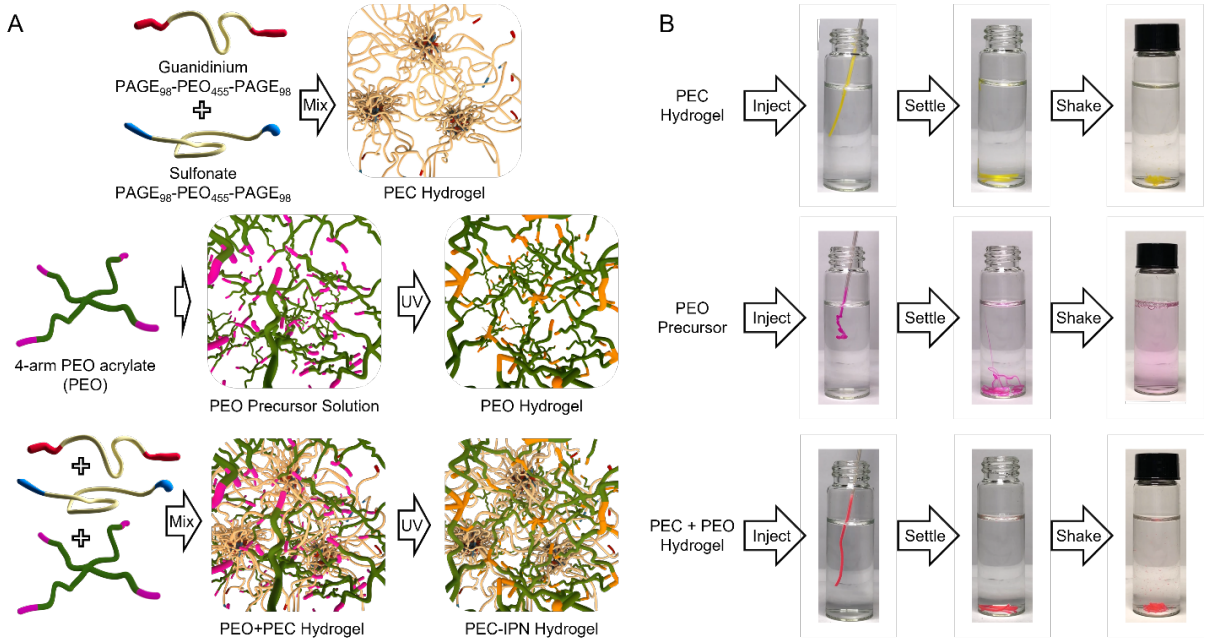

Figure 1. Schematic depiction of PEC, PEC+PEO and PEC-IPN hydrogels. (A) Schematics representing PEC (*row 1*), PEO (*row 2*), and PEC+PEO and PEC-IPN hydrogels (*row 3*). **(B)** Photographs demonstrating injectability and insolubility of PEC (*row 1*) and PEC+PEO (*row 3*) hydrogels in water. In contrast, the PEO precursor (*row 2*) dissolves in water readily. Dyes (Acid Yellow 73, Rhodamine B, and a combination of Acid Yellow 73 and Rhodamine B in rows 1, 2, and 3, respectively) were added in the hydrogels to aid visualization.

2.2. Structural Resilience of PEC Domains Against Inclusion of Polymers and Covalent Networks

Small angle X-ray scattering (SAXS) reveal the structural attributes of the PEC network comprising PEC domains interlinked with the neutral blocks of the bPEs. The PEC domains are composed of the charged blocks of the bPEs possess higher polymer concentration than the surroundings and include higher atomic number elements including nitrogen and sulfur, providing sufficient electron density contrast.[1, 4, 5] **Figure 2a** shows

representative one-dimensional SAXS intensity $I(q)$ as a function of wave vector q obtained from PEC hydrogels with increasing bPE concentrations (C_{bPE}, grey traces, see also **Figure S1A**). These SAXS spectra exhibit a broad primary peak near q = 0.02 Å^{-1} followed by secondary peaks at higher q values. The primary and the secondary peaks became more prominent with increasing C_{bPE}, indicating strengthening spatial correlations among the PEC domains. Yet, an absence of Bragg reflection peaks denote that the PEC domains remained in a disordered arrangement even in PEC hydrogels with C_{bPE} = 40 wt%.[1, 4, 5]

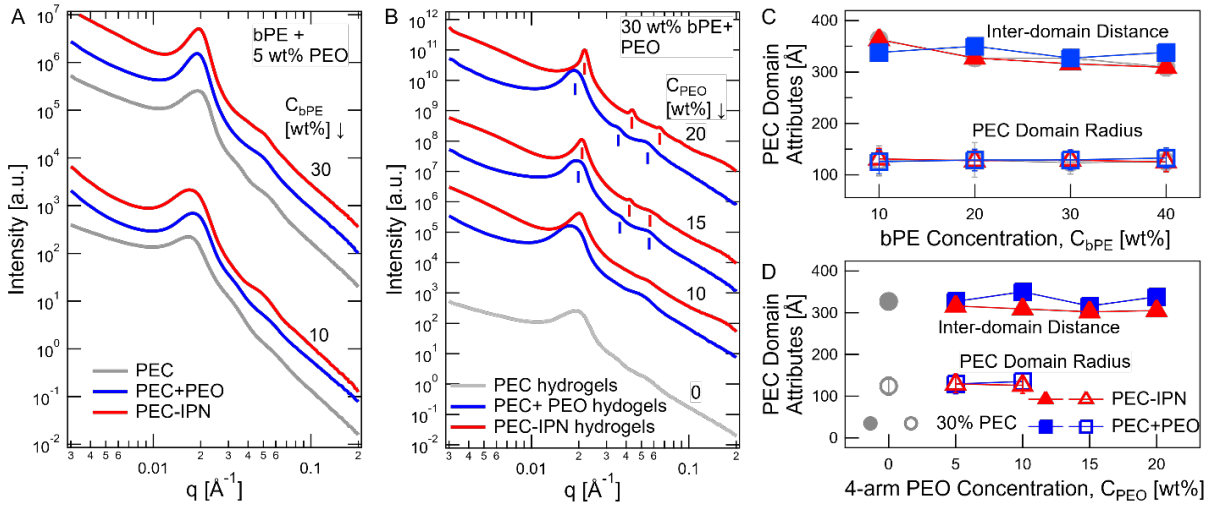

Figure 2. Representative SAXS scattering spectra and PEC domain attributes in PEC, PEC+PEO, and PEC-IPN hydrogels. (A) One-dimensional scattering intensity $I(q)$ as a function of wave vector q for PEC (grey), PEC+PEO (blue), and PEC-IPN (red) hydrogels with varying C_{bPE} from 10 wt% to 30 wt%. PEC+PEO, and PEC-IPN hydrogels also contained a constant C_{PEO} (= 5 wt%). **(B)** $I(q)$ spectra for PEC hydrogels with C_{bPE} = 30 wt%, and PEC+PEO, and PEC-IPN hydrogels with varying C_{PEO} (between 10 and 20 wt%) and constant C_{bPE} = 30 wt%. In the SAXS spectra for PEC+PEO, and PEC-IPN hydrogels with C_{PEO} = 15 wt% and 20 wt%, the small vertical bars indicate the positions of the Bragg scattering peaks. The secondary and the tertiary peaks appear at $2q^*$ and $3q^*$ with respect to the primary peak at q^*, denoting lamellar microstructure of the PEC domains. In both (A) and (B), $I(q)$ spectra are shifted vertically for clarity. **(C, D)** Inter-domain distance (d_{PEC}) and domain radius (R_{PEC}) as a function of C_{bPE} (C) and C_{PEO} (D) for PEC, PEC+PEO, and PEC-IPN hydrogels. In (C), C_{PEO} = 5 wt% while in (D), C_{bPE} = 30 wt%. See Supplementary Information Table S1 for peak assignments in (B).

Modeling $I(q)$ as a combination of a form factor $P(q)$ for polydisperse spheres and a hard sphere structure factor $S(q)$ as $I(q) \sim P(q)S(q)$, as shown in **Figure S2**, enabled estimation of the domain radius (R_{PEC}) and the characteristic inter-domain distance (d_{PEC}).[69, 70] The position of the primary $S(q)$ peak, q^*, represents the inverse inter-domain distance d_{PEC} as $d_{PEC} \sim 2\pi/q^*$.[69] R_{PEC} and d_{PEC} for the PEC hydrogels are shown in **Figure 2C** with grey symbols. Consistent with previous observations[5] that PEC domain size depends on the length of the charged block only while inter-domain correlation and distances are dictated by lengths of both the charged and the neutral blocks as well as C_{bPE}, R_{PEC} was found to be independent of C_{bPE} while d_{PEC} decreased progressively with increasing C_{bPE}.

Scattering from the PEC network persisted upon the inclusion of polymeric additives (PEO) and their subsequent crosslinking. **Figure 2A** highlights the similarity of the $I(q)$ spectra obtained from PEC hydrogels (grey traces) with PEC+PEO and PEC-IPN hydrogels containing 5 wt% PEO content (C_{PEO}), depicted by blue and red traces, respectively (see also **Figure S1A and S1B**). Correspondingly, both R_{PEC} and d_{PEC} for PEC hydrogels (grey symbols), PEC+PEO hydrogels (blue symbols) and PEC-IPN hydrogels (red symbols) evolved near identically with increasing C_{bPE} (**Figure 2C**).

Tuning the PEO content in the PEC+PEO or the PEC-IPN hydrogels enabled modulation of the PEC network nanostructure. Morphological transition and ordering of the PEC domains, signified by the appearance of sharp Bragg reflection peaks in the SAXS spectra in **Figure 2B** accompanied with a subtle decrease of d_{PEC} (**Figure 2D**) were observed with increasing C_{PEO} in both PEC+PEO and PEC-IPN hydrogels comprising C_{bPE} = 30 wt%. The relative positions of the primary (q_1), secondary (q_2) and tertiary (q_3) Bragg peaks as $q_1 : q_2 : q_3 \cong 1 : 2 : 3$ denote the presence of parallelly stacked lamellar PEC domains in the PEC network with $C_{PEO} \geq 15$ wt%.

Such morphological and ordering transitions, as well as reduction in domain spacing have been previously observed in PEC hydrogels with increasing PE concentration[1, 4, 5, 37] and have been hypothesized to arise from the compression of the neutral middle blocks beyond their equilibrium conformations.[5] Here, we expect macromolecular crowding by the 4-arm PEO chains or the covalent network to result in compression and loss of conformational entropy of the PEO midblocks, which in turn induces morphological and ordering transitions in PEC domains. It should be noted that the SAXS spectra shown here are representative of the nearly identical spectra obtained from multiple spots in each of the hydrogel samples, denoting the spatial homogeneity of the hydrogels.

PEC networks comprising weaker ammonium groups instead of strong guanidinium groups in the block polycations exhibit similar behaviors. Weaker electrostatic interactions between ammonium and sulfonate groups, however, resulted in larger PEC domains and faster equilibration of the PEC network. The resulting PEC hydrogels contained ordered PEC domains at $C_{bPE} \geq 30$ wt%. Addition of 5 wt% PEO did not disrupt either the disordered or the ordered PEC networks (**Figures S3A and S4**). Both disordered and ordered PEC networks, although, required smaller C_{PEO} to undergo ordering and morphological transition in PEC+PEO and PEC-IPN hydrogels (**Figure S3B**). Notwithstanding, the trends in d_{PEC} and R_{PEC} with varying C_{bPE} and C_{PEO} (**Figures S3C and S3D**) remained consistent with the trends shown in Figure 2.

2.3. Modulation of Shear Properties of PEC Hydrogels by Polymer Diluents and Interpenetrating Covalent Networks

PEC hydrogels exhibited frequency-independent storage and loss moduli (G' and G'', respectively) with $G' > G''$, for $C_{bPE} \geq 10$ wt%, indicating solid-like gels with an absence of terminal relaxation (grey symbols in **Figures 3A-C**).[4, 5] With increasing C_{bPE}, G' and G'' both increased before G' plateauing around 10 kPa, typical for PEC hydrogels (**Figure 3D**).[4, 5] Inclusion of PEO chains in the PEC hydrogels led to a decrease of both G' and G'' while conserving their frequency-independent behavior (blue symbols in **Figures 3A-C**). Subsequent crosslinking of the PEO chains led to a marked increase in the shear moduli of the resulting PEC-IPN hydrogels, even higher than the corresponding moduli for PEC hydrogels (red symbols in **Figures 3A-C**).

Figure 3F summarizes the evolution of shear response of PEC-IPN hydrogels with increasing C_{bPE} for a constant C_{PEO}. The influence of the covalent network on the shear moduli of PEC-IPN hydrogels was more pronounced when the covalent network served as the primary load-bearing network. When the shear moduli of PEC hydrogels with $C_{bPE} \leq 20$ wt% (**Figure 3D**) were smaller than of the 5 wt% covalent hydrogels (**Figure 3E** and **Figure S5**), the corresponding PEC-IPN hydrogels exhibited more than two-fold improvements in both G' and G'' as compared to the PEC hydrogels (**Figures 3D and 3F**, see also **Figures 3A** and **3B**). In contrast, only modest enhancements in moduli were achieved in PEC-IPN hydrogels with $C_{bPE} > 20$ wt%. Importantly, since the moduli of the covalent PEO network is directly proportional to the C_{PEO} (**Figure 3E**), PEO content in the PEC-IPN hydrogels can be harnessed as a facile route to tune their moduli. As an illustration, steady improvements in G'

and G'' of PEC-IPN hydrogels with C_{bPE} = 30 wt% were observed upon increasing C_{PEO} (**Figure 3C, 3D, 3G**, see also **Figure S6A-D**).

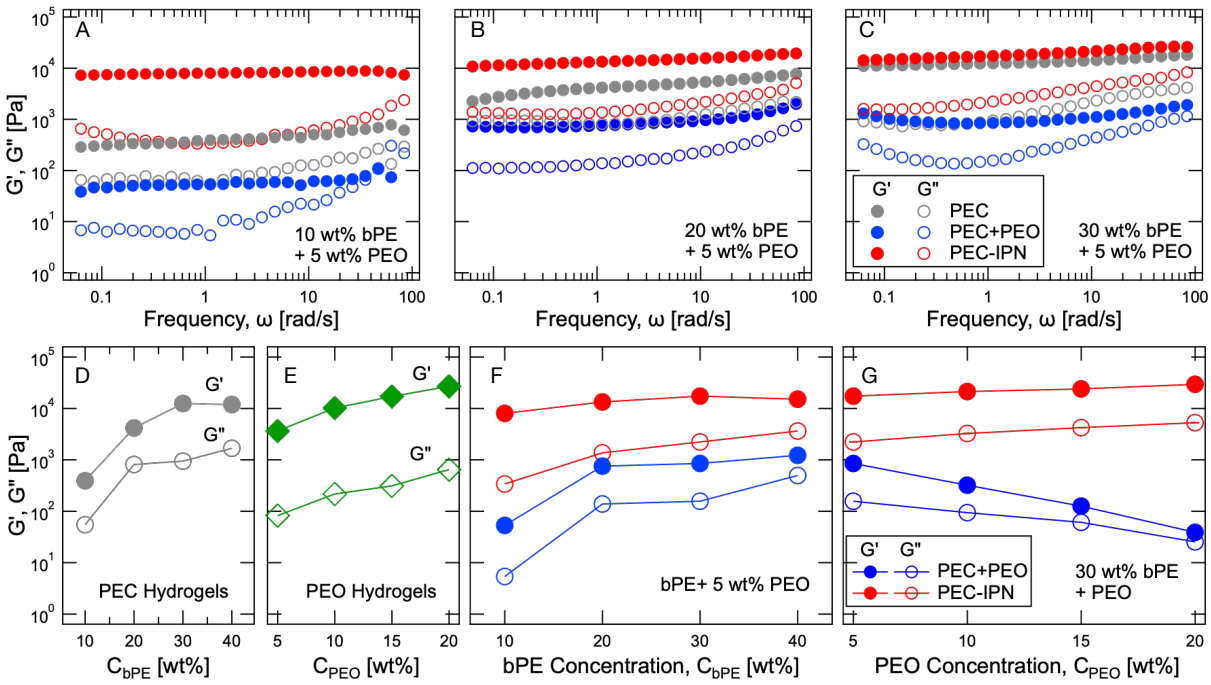

Figure 3. Modulations of shear strength of PEC+PEO and PEC-IPN hydrogels. (A-C) Storage (G') and loss (G'') moduli as a function of frequency (ω), measured by imposing oscillatory strain (strain amplitude γ = 0.3%) on PEC hydrogels (grey), PEC+PEO hydrogels (blue), and PEC-IPN hydrogels (red) with varying C_{bPE} and a constant C_{PEO}. **(D-G)** G' and G'' (at ω = 1.12 rad/s and γ = 0.3%) for PEC hydrogels with increasing C_{bPE} (D), PEO hydrogels with increasing C_{PEO} (E); and PEC+PEO hydrogels (blue) and PEC-IPN hydrogels (red) with increasing C_{bPE} and constant C_{PEO} = 5 wt% (F) and with increasing C_{PEO} and constant C_{bPE} = 30 wt% (G).

These moduli enhancements serve as an indicator of the interpenetrating nature of the PEC and the covalent networks and their synergistic contribution to shear strength of the resulting hybrid hydrogel. Interlacing of the two networks is hypothesized to hinder chain relaxation processes in both the networks (pullout and reinsertion of PE blocks in the PEC domains, chain fluctuations) resulting from a loss of their conformational freedom, leading to slower stress relaxation and higher moduli of the IPN hydrogels as compared to hydrogels comprising either of the components. Consequently, PEC-IPN hydrogels have superior shear strength which either PEC hydrogels or covalent hydrogels cannot achieve individually.

In contrast, PEC+PEO hydrogels exhibit a marked decrease in shear strength as compared to the PEC hydrogels (blue symbols in **Figures 3A-C and 3F**). Increasing PEO content in PEC+PEO hydrogels led to continuing reduction of G' and G'' (**Figure 3G**). We hypothesize that this reduction can be attributed to a reconfiguration of the PEC network by the 4-arm PEO chains.

Previously, it has been shown that self-assembly of symmetric, oppositely charged *ABA* triblock polyelectrolytes results in networks with a higher-than-expected fraction of *B* blocks forming bridges instead of loops, manifesting as gel formation at surprisingly low polymer concentrations.[3] Here, we argue that inclusion of 4-arm PEO chains induces macromolecular crowding, hindering bridge formation and promoting loop formation, reducing the network connectivity and reducing its shear moduli. Furthermore, the injectability of the PEC network containing precursor solutions can also be tuned precisely. The PEC+PEO hydrogels exhibit strong shear thinning characteristics (**Figure S7**) and the microstructure of the PEC networks recover quickly after strong shearing (**Figure S7E**),[71] resulting in facile injection and swift recovery of hydrogel elasticity post injection (**Figure 1B**, row 3).

We note that the PEC+PEO and the PEC-IPN hydrogels are both expected to be spatially uniform, and therefore, spatial inhomogeneities and phase separation are not expected to play a role in contributing to the observed decay of the PEC+PEO hydrogel moduli. The mixing protocols, comprising mixing of the 4-arm PEO and the block polyanions before the addition of the block polycations ensured uniform mixing of the polymers. Additionally, SAXS spectra collected from various locations in the hydrogel samples were identical, pointing towards spatially homogenous distribution of the PEC domains.

Similar trends were observed in PEC, PEC+PEO and PEC-IPN hydrogels comprising ammonium and sulfonated bPEs (**Figure S8**). These PEC hydrogels exhibited G' and G'' that were lower than the corresponding guanidinilated bPE-containing PEC hydrogels, and both moduli exhibited a maximum with increasing C_{bPE} owing to the morphological transitions of the PEC domains.[5] G' and $G"$ of these PEC hydrogels were lower even than that of 5 wt% 4-arm PEO hydrogels across C_{bPE} varying from 10 wt% to 40 wt%. Thus, distinct improvements in the moduli were achieved in PEC-IPN hydrogels as compared to the PEC hydrogels upon introduction of 5 wt% PEO (**Figure S8H**). And similar to variations depicted in Figure 3G, PEC-IPN and PEC+PEO hydrogel moduli varied continually with increasing C_{PEO} (**Figure S8I**).

2.4. Imparting Tensile Strength to the PEC Hydrogels by Interpenetration with Covalent Networks

Combining PEC networks with covalent networks also rendered tensile strength and extensibility to PEC-IPN hydrogels, characteristics that are inaccessible to PEC hydrogels, as illustrated in the representative stress-strain curves obtained from uniaxial tensile testing in **Figure 4**. The physically crosslinked PEC hydrogels do not possess tensile strength as the block polyelectrolyte chains can rearrange readily when subjected to tensile strain. In contrast, covalently crosslinked PEO hydrogels exhibit elasticity emerging from the finite extensibility of the polymer chains between the crosslinks. In PEC-IPN hydrogels, the covalent network is hypothesized to provide the tension points while the self-assembled domains that comprise the PEC network serve as energy-dissipating physical multi-linkages. The ultimate strength of the PEC-IPN hydrogels (C_{PEO} = 5 or 15 wt% + C_{bPE} = 30 wt%) was found to remain comparable to the corresponding covalent hydrogels, with minor loss of strength (**Figure S9A**). At the same time, as compared to corresponding PEO hydrogels, PEC-IPN hydrogels exhibit improvements in both extensibility and toughness (**Figure S9B and S9C**).

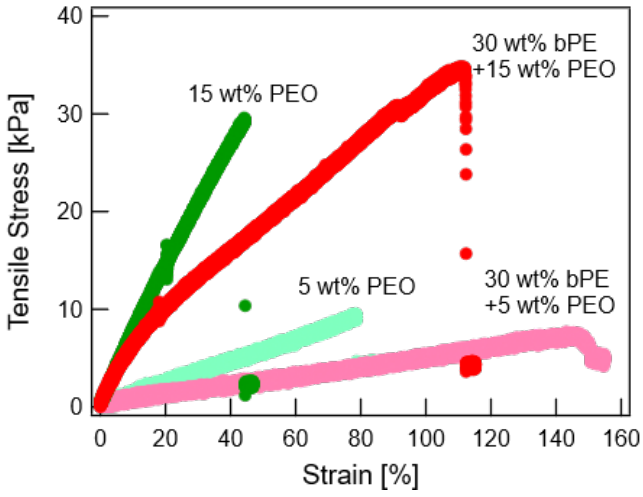

Figure 4. Imparting tensile strength to PEC network *via* PEC-IPN hydrogels. Representative stress curves as a function of strain for PEO and PEC-IPN hydrogels with C_{bPE} = 30 wt% and C_{PEO} = 5 or 15 wt%.

These improvements can be attributed to the reconfigurable nature of the PEC network, that enable network restructuring, thus promoting stress dissipation. The restructuring of the interpenetrating network proceeds through yielding of the PEC network and is further evident in the distinct two-step stress growth during uniaxial stretching of the

PEC-IPN hydrogels (**Figure 4**, see also **Figure S10**). At the same time, formation of the covalent network may be hindered partially by the PEC network, resulting in lower ultimate strength and higher extensibility. Similar enhancements in tensile performance were also noted upon replacing the guanidinium moieties with ammonium moieties in the bPEs comprising the PEC-IPN hydrogels (**Figure S11** and **Figure S12**).

2.5. Modulating the Response of PEC Hydrogels to Aqueous or Saline Environments

Figure 5 highlights the swelling characteristics of the PEC-IPN hydrogels. PEC-IPN hydrogels swelled more than their corresponding PEO hydrogels yet reached equilibrium within a few hours. Swelling in all hydrogels were found to plateau within 24 hours. The larger swelling of the PEC-IPN hydrogels could be attributed to the hydrophilic bPEs absorbing larger amounts of water, providing an excess osmotic pressure to further expand the interpenetrating polymer networks and partially hindered formation of the covalent network in the PEC-IPN hydrogels enabling its larger expansion. The swelling of PEC-IPN hydrogels could be tuned by varying C_{PEO}; the swelling ratio of PEC-IPN hydrogels increased by 18% upon increasing C_{PEO} from 5 wt% to 15 wt%. This is commensurate with the larger swelling of the 15 wt% PEO hydrogels as compared to the 5 wt% PEO hydrogels (**Figure 5**). Again, these are distinct improvements over the indefinite swelling of PEC hydrogels, ascribable to their physically crosslinked structure.

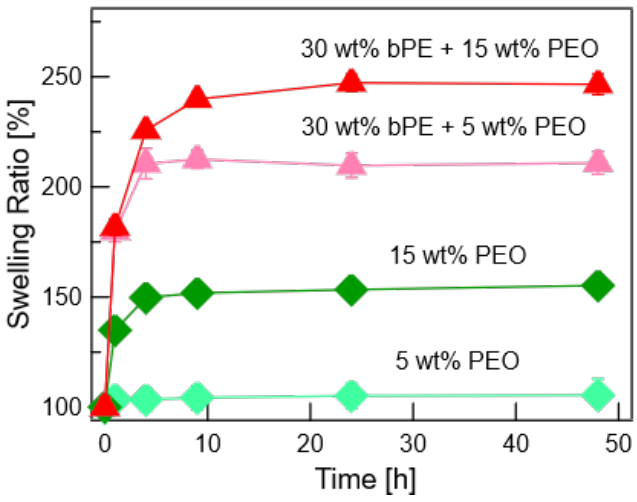

Figure 5. Controlling the swelling behavior of PEC network by interpenetration with covalent networks. The swelling of PEO and PEC-IPN hydrogels with C_{bPE} = 30 wt% and C_{PEO} = 5 or 15 wt%, as denoted by their weight gain with time.

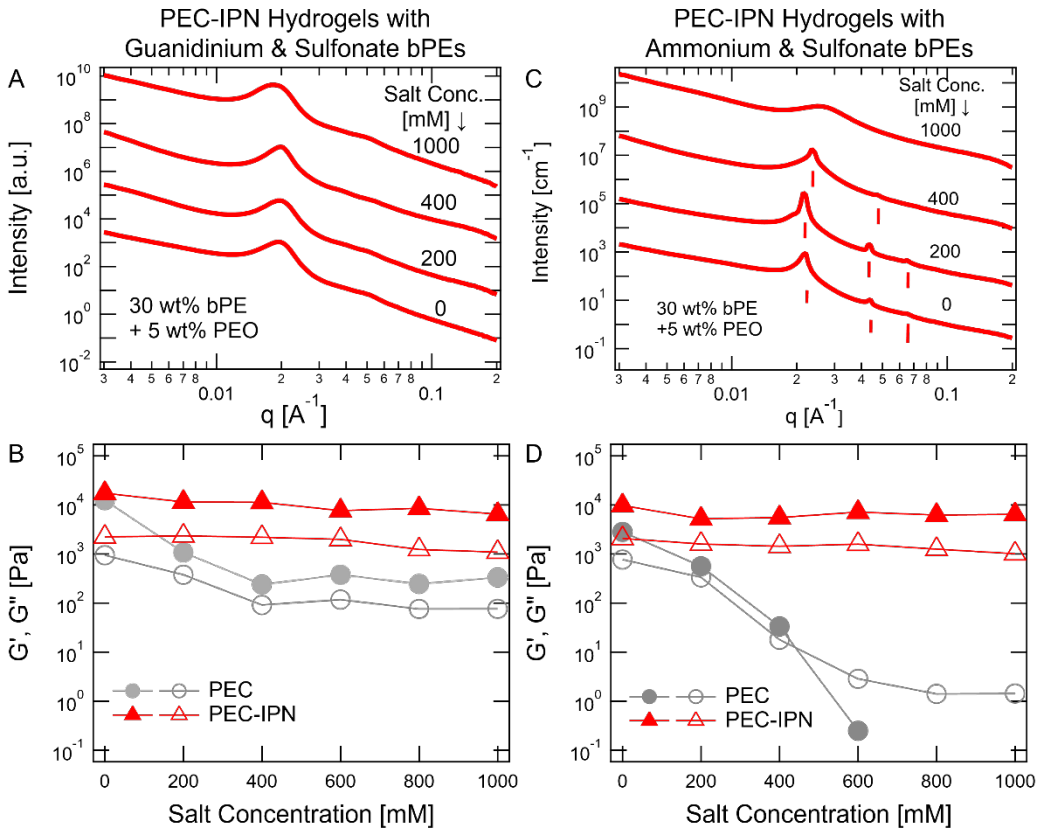

Figure 6. Evolution of microstructure and shear strength of PEC-IPN hydrogels in saline environments. (**A**) One-dimensional SAXS intensities $I(q)$ versus wave vector q and (**B**) the shear moduli (G' and $G"$), measured at $\omega = 1.12$ rad/s and $\gamma = 0.3\%$, as a function of salt concentration C_{salt} for PEC-IPN hydrogels ($C_{bPE} = 30$ wt% + $C_{PEO} = 5$ wt%) composed of bPEs functionalized with guanidinium and sulfonate moieties. In (B), corresponding G' and $G"$ data are also shown for PEC hydrogels ($C_{bPE} = 30$ wt%). (**C**) and (**D**) show data corresponding to (A) and (B), respectively for PEC-IPN hydrogels ($C_{bPE} = 30$ wt% + $C_{PEO} = 5$ wt%) and PEC hydrogels ($C_{bPE} = 30$ wt%) composed of bPEs functionalized with ammonium and sulfonate moieties. In (A) and (C), the $I(q)$ spectra were shifted vertically for clarity. See Supplementary Information Table S2 for peak assignments in (C).

PEC-IPN hydrogels also retained their mechanical strength upon exposure to salt. Introduction of salt resulted in progressive breakdown of the PEC network, evident from the broadening peaks in the SAXS spectra obtained from PEC-IPN hydrogels (C_{bPE} = 30 wt%, C_{PEO}= 5 wt%) with increasing salt concentrations (**Figures 6A and 6C**, see also **Figures S13A and S13D**). The influence of salt on the network microstructure was more evident in PEC networks containing ammonium functionalized bPEs (**Figure 6C**) as compared to guanidinilated bPEs (**Figure 6A**). Correspondingly, shear moduli of PEC hydrogels with

guanidinium moieties decreased by ~2 orders of magnitude upon increasing C_{salt} up till 600 mM (grey symbols in **Figure 6B**, see also **Figures S13B and S13C**) while the moduli of the PEC hydrogels with ammonium moieties decreased precipitously with increasing C_{salt}. In contrast, the corresponding PEC-IPN hydrogels exhibited far superior shear strength even when PEC network was disrupted, ascribable to the presence of the covalent network that sustains the shear response of the hydrogels in salty environments (red symbols in **Figures 6B and 6D**, see also **Figure S13**). Thus, the PEC-IPN hydrogels present a possibility of hydrogel design wherein ionic strength or pH can be varied to induce changes in network microstructure while retaining controlled moduli and swelling responses.

3. Conclusion and Implications in Biomaterials Development

In summary, we have demonstrated, for the first time, a facile approach to create PEC-IPN hydrogels composed of interpenetrating PEC networks (composed of oppositely charged block polyelectrolytes) and covalent networks (composed of photocrosslinked 4-arm PEO chains). PEC-IPN hydrogels are shown to possess superior shear and tensile properties which cannot be achieved by either of the individual networks. Moreover, the PEC-IPN hydrogels exhibit enhanced mechanical stability in salt environments and tunable swelling response.

The PEO chains and networks, at sufficiently high loadings, induce morphological and ordering transitions in the PEC domains, providing a handle to tune the PEC domain morphologies and arrangements. At the same time, interpenetration of the PEC network with the covalent network enables an independent modulation of the shear properties of the PEC network. PEC-IPN hydrogels with interpenetrating covalent and PEC networks featured $G' >$ 10 kPa, a regime rarely accessible by PEC hydrogels but is important for design of strong hydrogels and adhesives.

These improved features of the PEC-IPN hydrogels, as compared to PEC hydrogels, are highly desirable in numerous biomedical applications. For instance, the PEC-IPN hydrogels demonstrated here can serve as a model platform to establish routes for use of materials based on block polyelectrolyte self-assembly in biomedical applications as adhesives and scaffolding wherein a control over gel microstructure (and drug loading capacity), shear and tensile strength, and extensibility are sought.

In parallel, the platform can act as a facile method to address current challenges associated with the use of photocrosslinkable polymers in advanced materials and biomedicine. PEC hydrogels can serve as a protective scaffolding, preventing uncontrolled dilution of the precursor solution and avoiding material loss and functional deactivation in wet

environments. Moreover, the crosslinked gels can achieve higher moduli owing to the interpenetrating PEC network. Thus, combination of existing photocrosslinkable polymers and PEC hydrogels represents a promising one-pot solution that could be employed directly on application site without additional processing steps. These improvements can prove very beneficial for various applications where photocrosslinked hydrogels are employed, and especially applications wherein *in situ* crosslinking of the precursor polymers is sought.[72, 73] For instance, light-based biofabrication processes like extrusion-based 3D printing that face issues of low viscosity and weak structural integrity of the hydrogel precursor solution prior to photocrosslinking can benefit from inclusion of PEC networks into the 3-D printing inks. Such a combination can achieve initial shear strength, minimize loss of precursor from secondary flows, and promote inter-layer bonding, paving the way for high-resolution printing.[73] Similarly, drug-loaded hydrogels patches or adhesive tissue sealants that rely on chemical crosslinking of precursors *in situ* can also benefit from introduction of PEC networks in the precursor solution. The injectable precursor solutions in these applications typically possess a low viscosity and tend to perfuse from the site of injection into the surrounding tissue, leading to premature release of their drug cargo or weak and ineffective adhesion, respectively.[72] Incorporation of PEC networks can reinforce the mechanical properties of the injected hydrogel precursors, and thus mitigate the loss of precursor molecules and reduce their dosage.

4. Materials and Methods

Materials: Potassium (99.5% trace metals basis), naphthalene, poly(ethylene glycol) (M_n = 20,000 Da), 2,2-dimethoxy-2-phenylacetophenone, allyl glycidyl ether (AGE), calcium hydride, sodium 3-mercapto-1-propanesulfonate, technical grade (90%), 1H-pyrazole-1-carboxamidine hydrochloride (99%), cysteamine hydrochloride (≥ 98%), and Irgacure 2959 were obtained from Millipore Sigma. Tetrahydrofuran (THF) and dimethylformamide (DMF) were obtained from Fisher Scientific. 4-arm poly(ethylene oxide) acrylate (PEO, M_n = 20,000 Da, ≥ 95%) was obtained from JenKem Technology.

Block Polyelectrolyte Synthesis: Guanidinium, ammonium, and sulfonate functionalized poly(ally glycidyl ether)-*b*-poly(ethylene glycol)-*b*-poly(ally glycidyl ether) were synthesized following previously published protocols.[1] Briefly, AGE was purified by stirring with calcium hydride overnight and then processed by three freeze-pump-thaw cycles and distillation. Poly(ethylene glycol) (M_n = 20,000 Da) was dissolved in anhydrous THF and

titrated with potassium naphthalenide (0.4 M in anhydrous THF) until the solution acquired a light green color. AGE was added into the reaction mixture and stirred at 45 °C for 48 h. The polymerization reaction was terminated by addition of degassed methanol, and the final product poly(allyl glycidyl ether)-poly(ethylene glycol)-poly(allyl glycidyl ether) (PAGE-PEO-PAGE) was precipitated in hexane and filtered, followed by drying prior to further functionalization. The product was characterized by proton nuclear magnetic resonance (^{1}H NMR, 400 MHz), as shown in **Figure S14**. The degree of polymerization of the PAGE blocks was calculated from the relative heights of peaks in the NMR spectra and was determined to be $PAGE_{98}$-PEO_{455}-$PAGE_{98}$.

Thiol-ene reactions to functionalize the $PAGE_{98}$-PEO_{455}-$PAGE_{98}$ were carried out by dissolving the polymer and a functional thiol (5 equiv. per alkene) in a 1:1 volume ratio of DMF/water mixture in a 100 mL round bottom flask. After addition of the photoinitiator (2,2-dimethoxy-2-phenylacetophenone, 0.05 equiv. per alkene), the solution was irradiated with UV light (365 nm) for 6 hours under nitrogen atmosphere. Then, the final product solution was dialyzed against deionized water for 10 cycles of 8 hour each. The final ammonium or sulfonate functionalized polymers were obtained by lyophilization.[1, 5]

Guanidinium functionalized polymer was synthesized by dissolving appropriate amount of ammonium functionalized $PAGE_{98}$-PEO_{455}-$PAGE_{98}$ in phosphate-buffered saline (PBS) solution along with 1H-pyrazole-1-carboxamidine (4 equivalent per alkene). The pH of the solution was adjusted to 10 by using 10 m NaOH solution. The reaction mixture was stirred for 3 days, followed by dialysis against deionized water for 10 cycles of 8 hours each. The final guanidinium functionalized polymers were obtained by lyophilization. All functionalized products were characterized by ^{1}H NMR (400 MHz) (**Figure S14**).[1, 5]

Preparation of PEC, PEC+PEO, and PEC-IPN Hydrogels: 50 wt% stock solutions of the cationic and anionic block polyelectrolytes were prepared by mixing, for example, 500 mg of the polymers with 1 mL of deionized water. PEC hydrogels were prepared by the protocol: an appropriate amount of block polycation stock solution was mixed with deionized water. Then, an appropriate amount of the block polyanion stock solution was added to the solution. The polymers were mixed in proportions such that the molar charge ratio of cationic and anionic groups was 1:1.

PEC+PEO hydrogels were prepared by mixing the block polycation stock solution with an aqueous solution of PEO and photoinitiator Irgacure 2959. Subsequently, the block polyanion stock solution was added. Each addition step was followed by vortex mixing to

homogenize the mixtures. The polymers were mixed in proportions such that the molar charge ratio of cationic and anionic groups was 1:1.

PEC-IPN hydrogels were prepared by exposing PEC+PEO hydrogels to UV radiation (302 nm, 8 W) for 5 minutes.

Small-angle X-ray scattering (SAXS) Measurement: Small-angle X-ray scattering measurements were performed at beamline 12-ID-B at the Advanced Photon Source, Argonne National Laboratory with 13 keV X-rays. The sample-to-detector distance was set at 4 meters, corresponding to a wave vector (q) range of 0.0002 Å^{-1} to 0.5 Å^{-1}. PEC and PEC+PEO hydrogels were loaded into holes (3 mm diameter) in 4 mm thick aluminum strips using a positive displacement pipet and sealed on both side with Kapton tape to avoid water evaporation. PEC-IPN hydrogels were prepared by loading PEC+PEO hydrogels in the aluminum strips and followed by 5 minutes UV light exposure and then sealed by Kapton tape. The X-ray exposure time was set at 0.1 second. All experiments were performed at room temperature. The two-dimensional scattering data were converted into one-dimensional data (I_{sample}) by using the matSAXS package. Sample scattering intensity was acquired by subtracting the appropriately scaled background (solvent) scattering intensity ($I_{solvent}$) from the measured scattering intensity, $I(q) = I_{sample} - \alpha I_{solvent}$, with α being the scaling parameter.[5] $P(q)$ and $S(q)$ fits to the $I(q)$ data were carried out using the Irena package[74] in Igor Pro.

Rheological Measurements: Oscillatory rheological measurements were performed on an Anton Paar MCR 302 rheometer using a parallel plate (diameter: 8 mm, gap size: 0.7 mm) fixture for PEC-IPN hydrogels and a cone and plate (diameter: 10 mm, cone angle: 2°) fixture for PEC and PEC+PEO hydrogels. An appropriate amount of PEC or PEC+PEO hydrogel samples was placed on the lower plate, and excess sample volume was trimmed after reaching the appropriate gap between the cone and the plate. PEC-IPN hydrogel samples were prepared by pipetting 70 µL of PEC+PEO hydrogels into a cylindrical polydimethylsiloxane (PDMS) mold (diameter: 8 mm, height: 1.5 mm) and irradiating the hydrogels with UV radiation for 5 minutes. The crosslinked hydrogel samples thus obtained were placed between the parallel plates of the rheometer fixture. All samples were pre-sheared by employing an oscillatory shear at $\gamma = 0.3\%$ for 40 minutes to reach equilibrium. Amplitude sweeps, with strain amplitude γ ranging from 0.01 - 100% (**Figure S15**) were carried out at frequency $\omega = 1$ rad/s to assess the linear viscoelastic (LVE) regime. Frequency

sweeps ($\omega = 0.01$-100 Hz) were performed at $\gamma = 0.3\%$, staying within the LVE regime. A solvent trap was employed to minimize water evaporation. All rheology data were acquired at 25 °C.

Tensile Tests: All tensile measurements were conducted on an Instron 5542 mechanical tester. PEO and PEC-IPN hydrogels were prepared by pipetting 80 microliters of the precursor solution into a rectangular PDMS mold (12 mm × 5 mm × 1.5 mm) and exposed to UV radiation for photocrosslinking. The crosslinked hydrogels were affixed to the machine tension grips with double-sided tape. The extension rate was set to 1 mm/min, and the stress-strain data were continuously collected until the fracture of samples. The tensile properties were estimated by averaging data obtained from at least 3 hydrogel samples.

Swelling Ratio: PEO and PEC-IPN hydrogel samples were prepared by pipetting 60 microliter of precursor solution (PEO solution or PEC+PEO hydrogels) into a cylindrical PDMS mold (diameter: 5 mm, height: 3 mm) and irradiating with UV radiation for 5 minutes. The hydrogel samples were transferred into a 24-well culture plate filled with deionized water. After 0, 1, 4, 9, 24, and 48 h, the hydrogel samples were weighed after carefully removing residual water from the surface. The swelling ratio of hydrogels was calculated as

$$Swelling\ Ratio = \frac{m_t}{m_0} \times 100\%$$

Here m_t is the weight of the hydrogel at time t (hour), m_0 is the initial weight. The swelling ratio was calculated by averaging the data of at least 3 samples.

Supporting Information

Supporting Information is available from the Wiley Online Library or from the author.

Acknowledgements

This research was supported by National Science Foundation under grant No. DMR-2048285. This research uses the facility of the Advanced Photon Sources, a U.S. Department of Energy (DOE) Office of Science User Facility operated for the DOE Office of Science by Argonne National Laboratory under GUP 66300. Support for T. G. and U. S. was provided by the Deutsche Forschungsgemeinschaft (DFG, German Research Foundation) under Germany's Excellence Strategy via the Excellence Cluster 3D Matter Made to Order (EXC-2082/1 – 390761711) and by the Bundesministerium für Bildung und Forschung (BMBF) by the KMU-

NetC 3D-Bio-Net (FKZ 03VNE1034D). T.G. acknowledges financial support by the Karlsruhe House of Young Scientists (KHYS) and is funded by a Kekulé Fellowship of the Chemical Industry Fund. D. L. acknowledges the access to the Instron 5542 tester by Prof. Nasim Annabi and her research group.

References

[1] J. N. Hunt, K. E. Feldman, N. A. Lynd, J. Deek, L. M. Campos, J. M. Spruell, B. M. Hernandez, E. J. Kramer, C. J. Hawker, *Advanced Materials* **2011**, 23, 2327.

[2] M. Lemmers, J. Sprakel, I. K. Voets, J. van der Gucht, M. A. Cohen Stuart, *Angewandte Chemie* **2010**, 122, 720.

[3] S. Srivastava, M. Andreev, A. E. Levi, D. J. Goldfeld, J. Mao, W. T. Heller, V. M. Prabhu, J. J. de Pablo, M. V. Tirrell, *Nature Communications* **2017**, 8, 14131.

[4] D. V. Krogstad, N. A. Lynd, S.-H. Choi, J. M. Spruell, C. J. Hawker, E. J. Kramer, M. V. Tirrell, *Macromolecules* **2013**, 46, 1512.

[5] S. Srivastava, A. E. Levi, D. J. Goldfeld, M. V. Tirrell, *Macromolecules* **2020**, 53, 5763.

[6] M. Lemmers, E. Spruijt, L. Beun, R. Fokkink, F. Leermakers, G. Portale, M. A. C. Stuart, J. van der Gucht, *Soft Matter* **2012**, 8, 104.

[7] M. Lemmers, E. Spruijt, S. Akerboom, I. K. Voets, A. C. van Aelst, M. A. Cohen Stuart, J. van der Gucht, *Langmuir* **2012**, 28, 12311.

[8] D. V. Krogstad, S.-H. Choi, N. A. Lynd, D. J. Audus, S. L. Perry, J. D. Gopez, C. J. Hawker, E. J. Kramer, M. V. Tirrell, *The Journal of Physical Chemistry B* **2014**, 118, 13011.

[9] D. V. Krogstad, N. A. Lynd, D. Miyajima, J. Gopez, C. J. Hawker, E. J. Kramer, M. V. Tirrell, *Macromolecules* **2014**, 47, 8026.

[10] H. Cui, X. Zhuang, C. He, Y. Wei, X. Chen, *Acta Biomaterialia* **2015**, 11, 183.

[11] C. M. Papadakis, C. Tsitsilianis, *Gels* **2017**, 3, 3.

[12] J.-M. Kim, T.-Y. Heo, S.-H. Choi, *Macromolecules* **2020**, 53, 9234.

[13] D. Seliktar, *Science* **2012**, 336, 1124.

[14] Y. S. Zhang, A. Khademhosseini, *Science* **2017**, 356, eaaf3627.

[15] K. Y. Lee, D. J. Mooney, *Chemical Reviews* **2001**, 101, 1869.

[16] K. T. Nguyen, J. L. West, *Biomaterials* **2002**, 23, 4307.

[17] A. Khademhosseini, R. Langer, *Biomaterials* **2007**, 28, 5087.

[18] H. Wang, S. C. Heilshorn, *Advanced Materials* **2015**, 27, 3717.

[19] M. Mehdizadeh, J. Yang, *Macromolecular Bioscience* **2013**, 13, 271.

[20] C. W. Peak, J. J. Wilker, G. Schmidt, *Colloid and Polymer Science* **2013**, 291, 2031.

[21] F. Scognamiglio, A. Travan, I. Rustighi, P. Tarchi, S. Palmisano, E. Marsich, M. Borgogna, I. Donati, N. de Manzini, S. Paoletti, *Journal of Biomedical Materials Research Part B: Applied Biomaterials* **2016**, 104, 626.
[22] P. Kord Forooshani, B. P. Lee, *Journal of Polymer Science Part A: Polymer Chemistry* **2017**, 55, 9.
[23] V. Bhagat, M. L. Becker, *Biomacromolecules* **2017**, 18, 3009.
[24] J. Li, A. Celiz, J. Yang, Q. Yang, I. Wamala, W. Whyte, B. Seo, N. Vasilyev, J. Vlassak, Z. Suo, *Science* **2017**, 357, 378.
[25] X. Chen, H. Yuk, J. Wu, C. S. Nabzdyk, X. Zhao, *Proceedings of the National Academy of Sciences* **2020**, 117, 15497.
[26] Y. Gao, X. Han, J. Chen, Y. Pan, M. Yang, L. Lu, J. Yang, Z. Suo, T. Lu, *Proceedings of the National Academy of Sciences* **2021**, 118.
[27] T. R. Hoare, D. S. Kohane, *Polymer* **2008**, 49, 1993.
[28] P. Kesharwani, A. Bisht, A. Alexander, V. Dave, S. Sharma, *Journal of Drug Delivery Science and Technology* **2021**, 66, 102914.
[29] J. Li, D. J. Mooney, *Nature Reviews Materials* **2016**, 1, 1.
[30] R. Dimatteo, N. J. Darling, T. Segura, *Advanced Drug Delivery Reviews* **2018**, 127, 167.
[31] M. M. Pakulska, K. Vulic, R. Y. Tam, M. S. Shoichet, *Advanced Materials* **2015**, 27, 5002.
[32] C. Yang, Z. Suo, *Nature Reviews Materials* **2018**, 3, 125.
[33] J. Deng, H. Yuk, J. Wu, C. E. Varela, X. Chen, E. T. Roche, C. F. Guo, X. Zhao, *Nature Materials* **2020**, 1.
[34] Y. Cao, R. Mezzenga, *Nature Food* **2020**, 1, 106.
[35] J. Li, X. Jia, L. Yin, *Food Reviews International* **2021**, 37, 313.
[36] J. Jiang, E.-Q. Chen, S. Yang, *Journal of Chemical Physics* **2021**, 154, 144903.
[37] D. J. Audus, J. D. Gopez, D. V. Krogstad, N. A. Lynd, E. J. Kramer, C. J. Hawker, G. H. Fredrickson, *Soft Matter* **2015**, 11, 1214.
[38] D. J. Audus, G. H. Fredrickson, in *Materials for Energy Infrastructure*, Springer, Singapore **2016**.
[39] R. Staňo, P. Košovan, A. Tagliabue, C. Holm, *Macromolecules* **2021**, 54, 4769.
[40] T. L. Sun, T. Kurokawa, S. Kuroda, A. B. Ihsan, T. Akasaki, K. Sato, M. A. Haque, T. Nakajima, J. P. Gong, *Nature Materials* **2013**, 12, 932.
[41] R. Shi, T. L. Sun, F. Luo, T. Nakajima, T. Kurokawa, Y. Z. Bin, M. Rubinstein, J. P. Gong, *Macromolecules* **2018**, 51, 8887.

[42] T. L. Sun, K. Cui, J. P. Gong, *Polymer Science, Series C* **2017**, 59, 11.
[43] H. Fan, J. Wang, J. P. Gong, *Advanced Functional Materials* **2021**, 31.
[44] S. Li, H. Pan, Y. Wang, J. Sun, *Journal of Materials Chemistry A* **2020**, 8, 3667.
[45] F. Luo, T. L. Sun, T. Nakajima, T. Kurokawa, Y. Zhao, K. Sato, A. B. Ihsan, X. Li, H. Guo, J. P. Gong, *Advanced Materials* **2015**, 27, 2722.
[46] G. Li, G. Zhang, R. Sun, C.-P. Wong, *Polymer* **2016**, 107, 332.
[47] Q. Liu, Z. Dong, Z. Ding, Z. Hu, D. Yu, Y. Hu, N. Abidi, W. Li, *ACS Sustainable Chemistry & Engineering* **2018**, 6, 7052.
[48] M. Lemmers, I. K. Voets, M. A. C. Stuart, J. Van Der Gucht, *Soft Matter* **2011**, 7, 1378.
[49] A. L. Z. Lee, Z. X. Voo, W. Chin, R. J. Ono, C. Yang, S. Gao, J. L. Hedrick, Y. Y. Yang, *ACS Applied Materials & Interfaces* **2018**, 10, 13274.
[50] S. Gao, A. Holkar, S. Srivastava, *Polymers* **2019**, 11, 1097.
[51] J. R. Magana, C. Sproncken, I. K. Voets, *Polymers* **2020**, 12, 1953.
[52] F. Chen, M. H. Stenzel, *Australian Journal of Chemistry* **2018**, 71, 768.
[53] J. M. Horn, R. A. Kapelner, A. C. Obermeyer, *Polymers* **2019**, 11, 578.
[54] S. Shah, L. Leon, *Current Opinion in Colloid & Interface Science* **2021**, 53, 101424.
[55] D. E. Discher, D. J. Mooney, P. W. Zandstra, *Science* **2009**, 324, 1673.
[56] A. J. Engler, S. Sen, H. L. Sweeney, D. E. Discher, *Cell* **2006**, 126, 677.
[57] D. E. Discher, P. Janmey, Y.-l. Wang, *Science* **2005**, 310, 1139.
[58] H. Kamata, X. Li, U.-i. Chung, T. Sakai, *Advanced Healthcare Materials* **2015**, 4, 2360.
[59] H. Yang, S. Ghiassinejad, E. van Ruymbeke, C.-A. Fustin, *Macromolecules* **2020**, 53, 6956.
[60] A. P. Dhand, J. H. Galarraga, J. A. Burdick, *Trends in Biotechnology* **2021**, 39, 519.
[61] D. J. Waters, K. Engberg, R. Parke-Houben, C. N. Ta, A. J. Jackson, M. F. Toney, C. W. Frank, *Macromolecules* **2011**, 44, 5776.
[62] E. S. Dragan, *Chemical Engineering Journal* **2014**, 243, 572.
[63] D. Myung, D. Waters, M. Wiseman, P. E. Duhamel, J. Noolandi, C. N. Ta, C. W. Frank, *Polymers for Advanced Technologies* **2008**, 19, 647.
[64] M. S. Silverstein, *Polymer* **2020**, 207, 122929.
[65] H. Wu, J. M. Ting, B. Yu, N. E. Jackson, S. Meng, J. J. de Pablo, M. V. Tirrell, *ACS Macro Letters* **2020**, 9, 1674.
[66] R. Takahashi, T. Narayanan, S. Yusa, T. Sato, *Macromolecules* **2022**, 55, 684.
[67] M. Amann, J. S. Diget, J. Lyngsø, J. S. Pedersen, T. Narayanan, R. Lund, *Macromolecules* **2019**, 52, 8227.

[68] X. Liu, M. Haddou, I. Grillo, Z. Mana, J.-P. Chapel, C. Schatz, *Soft Matter* **2016**, 12, 9030.

[69] A. Guinier, G. Fournet, *Small-angle Scattering of X-rays*, John Wiley and Sons, New York, NY **1955**.

[70] O. Kratky, G. Porod, *Small angle X-ray scattering*, Vol. 68, Academic Press, New York, NY **1982**.

[71] D. V. Krogstad, *Investigating the Structure-Property Relationships of Aqueous Self-Assembled Materials*, University of California, Santa Barbara **2012**.

[72] S. Bian, Z. Zheng, Y. Liu, C. Ruan, H. Pan, X. Zhao, *Journal of Materials Chemistry B* **2019**, 7, 6488.

[73] J. M. Townsend, E. C. Beck, S. H. Gehrke, C. J. Berkland, M. S. Detamore, *Progress in Polymer Science* **2019**, 91, 126.

[74] J. Ilavsky, P. R. Jemian, *Journal of Applied Crystallography* **2009**, 42, 347-353.

Hydrogels composed of interpenetrating polyelectrolyte complex network and covalently crosslinked network demonstrate substantial improvements in mechanical strength, toughness, and swelling performance while conserving the microstructure of the PEC network.

Defu Li, Tobias Göckler, Ute Schepers, Samanvaya Srivastava*

Polyelectrolyte Complex-Covalent Interpenetrating Polymer Network Hydrogels

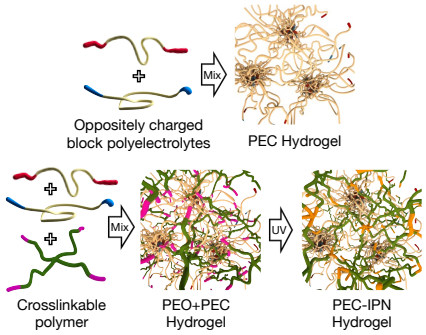

Supporting Information

Polyelectrolyte Complex-Covalent Interpenetrating Polymer Network Hydrogels

*Defu Li, Tobias Göckler, Ute Schepers, Samanvaya Srivastava**

Contents:

Figure S1-S15

Table S1-S4

Movies SM1-SM3

Supplementary Figures

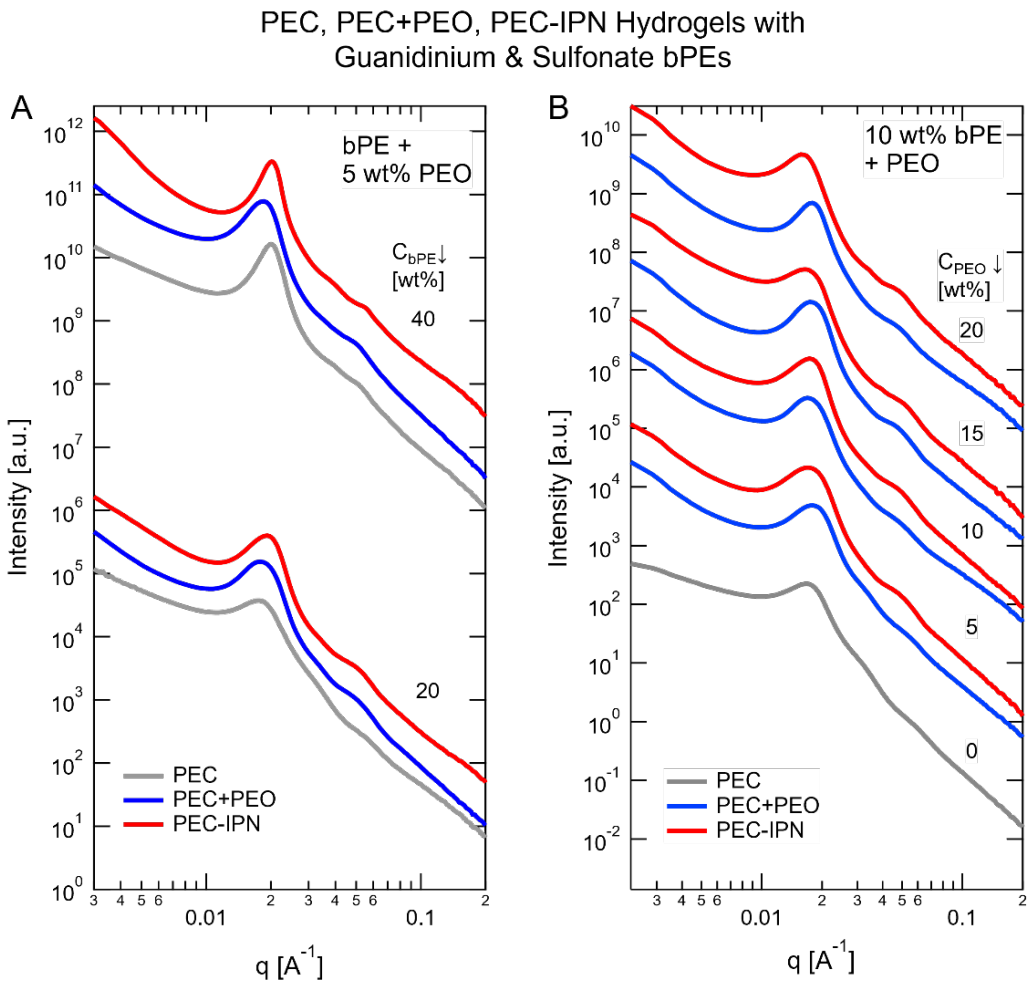

Figure S1. Representative SAXS scattering spectra in PEC, PEC+PEO, PEC-IPN hydrogels consisting of guanidinium and sulfonate functionalized polyelectrolytes. **(A)** 1-D scattering intensity $I(q)$ as a function of wave factor q for PEC (grey), PEC+PEO (blue), and PEC-IPN (red) hydrogels with a fixed C_{PEO} (= 5 wt%) and varying C_{bPE} from 20 wt% to 40 wt%. **(B)** $I(q)$ spectra for PEC hydrogels (with C_{bPE}= 10 wt%), PEC+PEO, and PEC-IPN hydrogels with varying C_{PEO} from 5 wt% to 20 wt%. $I(q)$ spectra are shifted vertically for clarity.

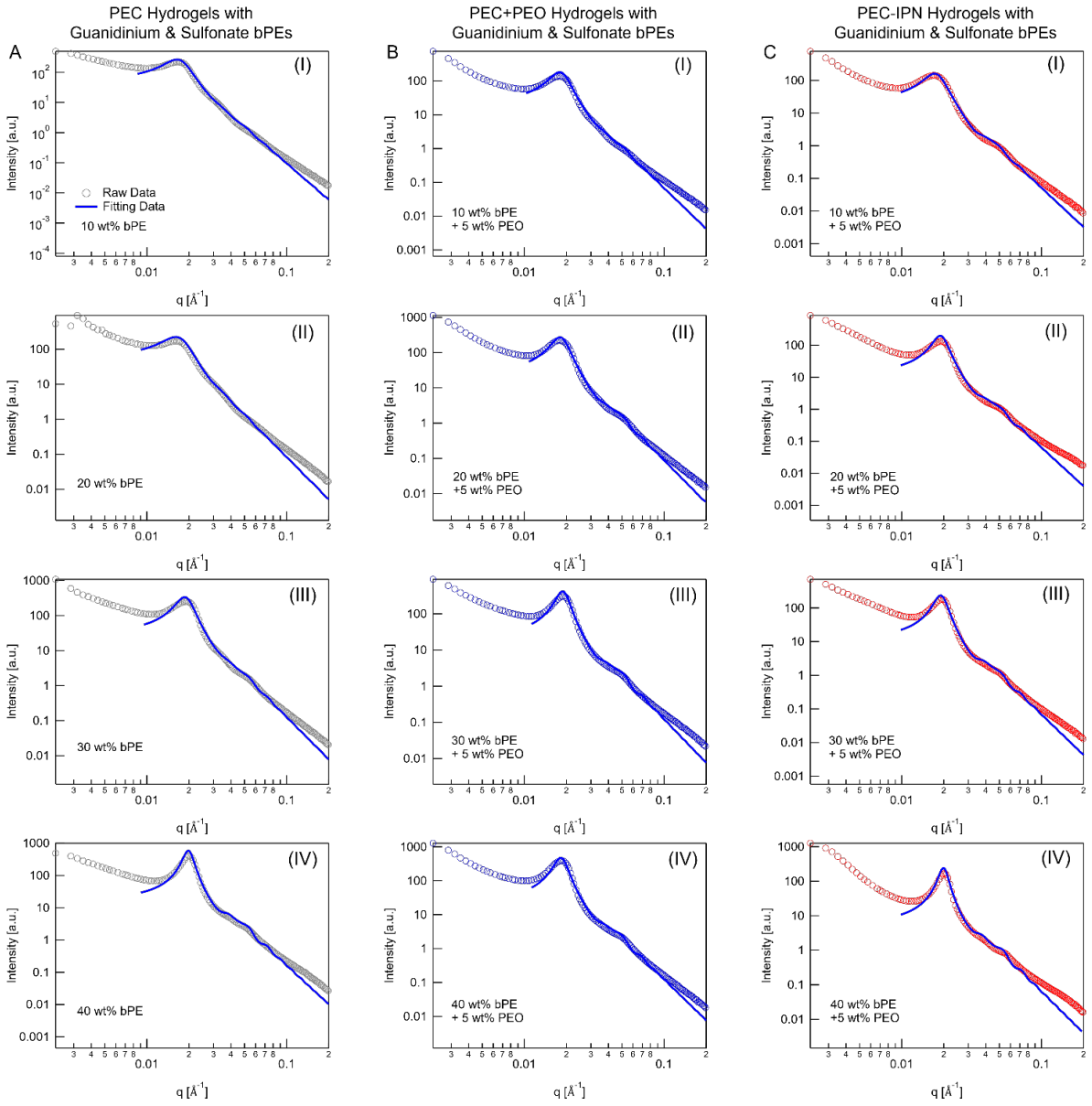

Figure S2. Representative fitting curves of PEC domain core radius of **(A, I-IV)** PEC hydrogels with varying C_{bPE} from 10 wt% to 40 wt%, **(B, I-IV)** PEC+PEO hydrogels and **(C, I-IV)** PEC-IPN hydrogels with a fixed C_{PEO} (= 5 wt%) and varying C_{bPE} from 10 wt% to 40 wt%. The fitting curves were modeled by polydisperse spheroid form factor and hard-sphere structure factor.

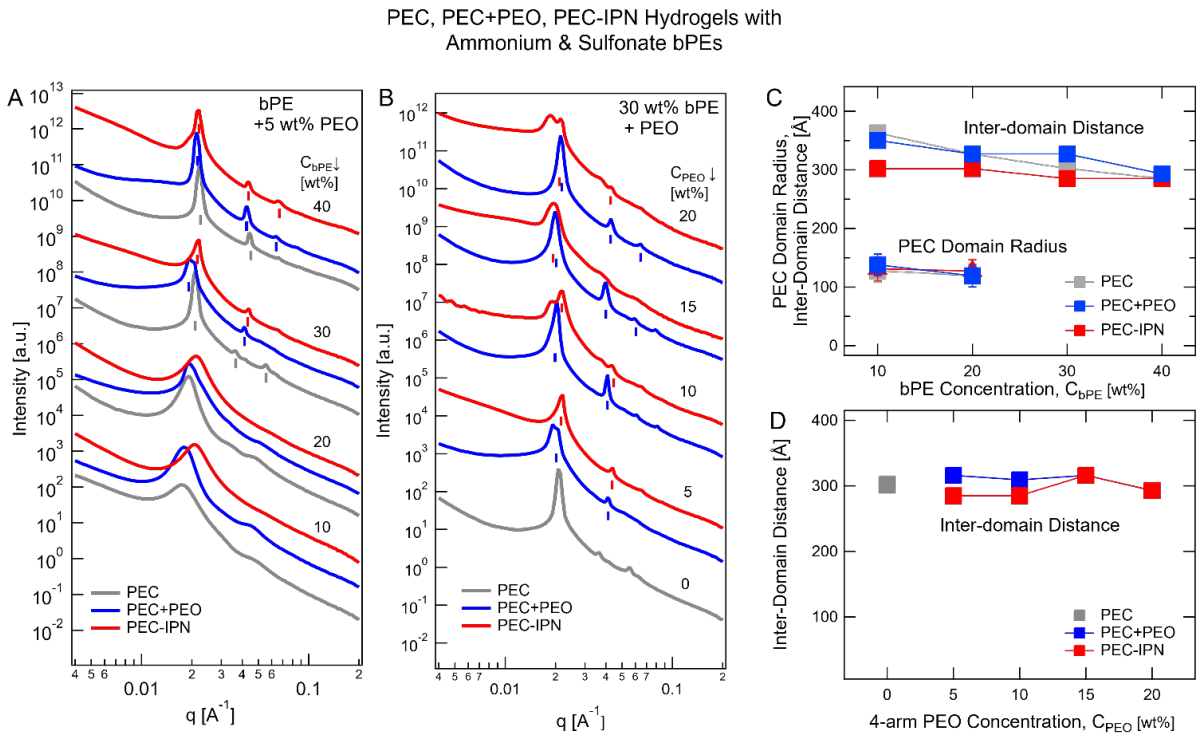

Figure S3. **SAXS scattering spectra and PEC domain attributes in PEC, PEC+PEO, PEC-IPN hydrogels with polyelectrolytes functionalized with ammonium and sulfonate groups**. **(A)** 1-D scattering intensity $I(q)$ as a function of wave vector q for PEC (grey), PEC+PEO (blue), and PEC-IPN (red) hydrogels with varying C_{bPE} from 10 wt% to 40 wt%. PEC+PEO and PEC-IPN hydrogels also contained a fixed C_{PEO} (= 5 wt%). **(B)** $I(q)$ spectra for PEC hydrogels with $C_{bPE} = 30$ wt%, and PEC+PEO, and PEC-IPN hydrogels with varying C_{PEO} (between 5 wt% and 20 wt%) and constant $C_{bPE} = 30$ wt%. The small vertical bars indicate the positions of the Bragg scattering peaks. With respect to the primary peak (at q^*), the secondary and the tertiary peaks appear at $2q^*$ and $3q^*$, denoting lamellar microstructure of the PEC domains. In (A) and (B), $I(q)$ spectra are shifted vertically for clarity. **(C, D)** Inter-domain distance (d_{PEC}) and domain radius (R_{PEC}) as a function of C_{bPE} (C) and C_{PEO} (D) for PEC, PEC+PEO, and PEC-IPN hydrogels. In (C), $C_{PEO} = 5$ wt%, while in (D), $C_{bPE} = 30$ wt%. See Supplementary Information Tables S3 and S4 for peak assignments in (C) and (D).

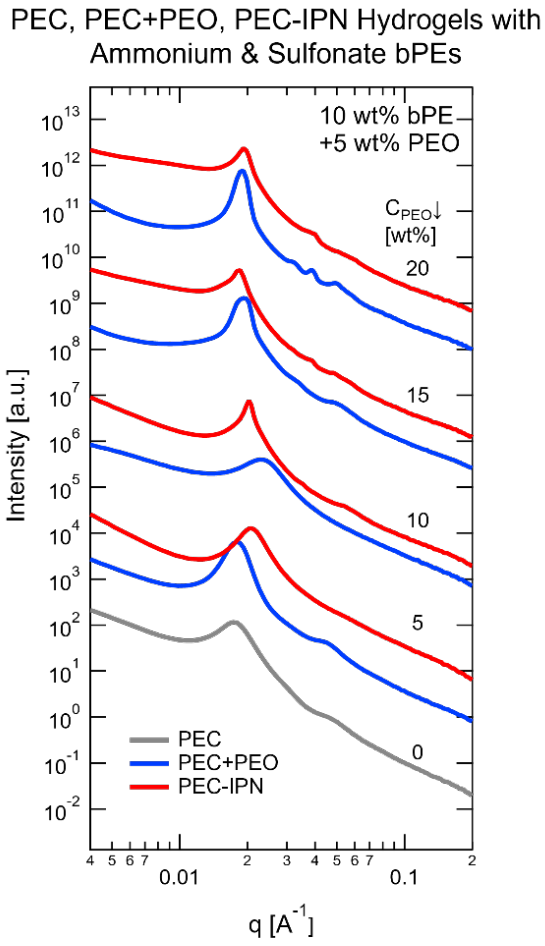

Figure S4. **SAXS scattering spectra in PEC, PEC+PEO, and PEC-IPN hydrogels.** 1-D scattering intensity $I(q)$ as a function of wave vector q for PEC (grey), PEC+PEO (blue), and PEC-IPN (red) hydrogels with a fixed C_{bPE} (= 10 wt%) and varying C_{PEO} from 5 wt% to 20 wt%. $I(q)$ spectra are shifted vertically for clarity.

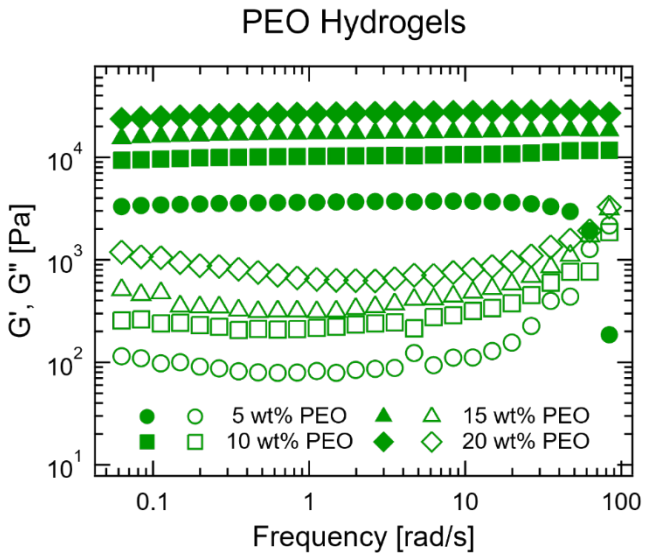

Figure S5. Shear strength of PEO hydrogels. Storage (G') and loss (G'') moduli as a function of frequency (ω) for PEO hydrogels with varying C_{PEO} from 5 wt% to 20 wt%.

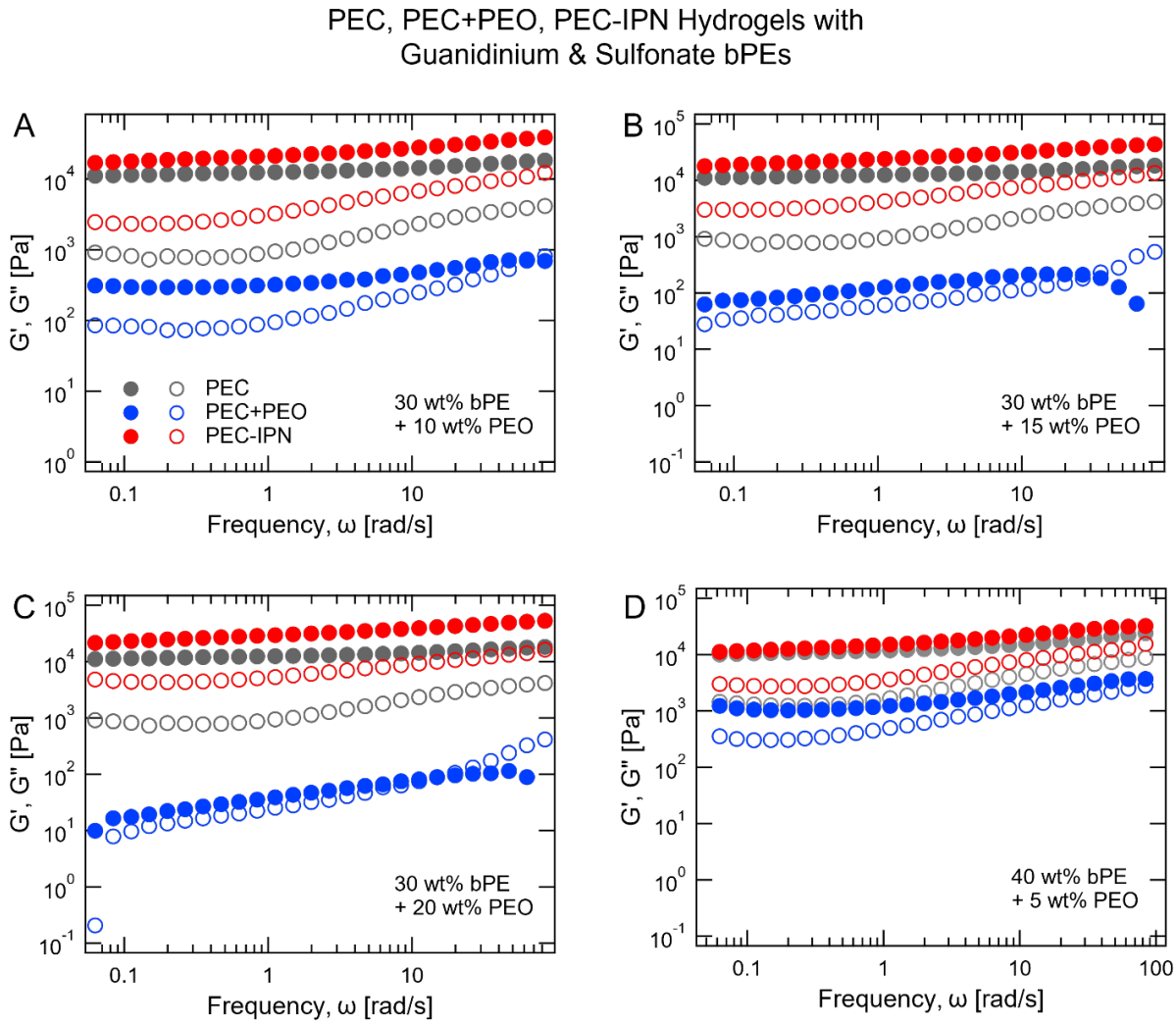

Figure S6. Shear strength of PEC, PEC+PEO, PEC-IPN hydrogels. (A-C) Storage (G') and loss (G'') moduli as a function of frequency (ω) for PEC hydrogels (grey), PEC+PEO hydrogels (blue), and PEC-IPN hydrogels (red) with varying C_{PEO} from 10 wt% to 20 wt% and a constant C_{bPE} (= 30 wt%). **(D)** $G'$and (G") as a function of ω for PEC (with C_{bPE} = 40 wt%), PEC+PEO, and PEC-IPN hydrogels with C_{bPE} = 40 wt% and C_{PEO} = 5 wt%.

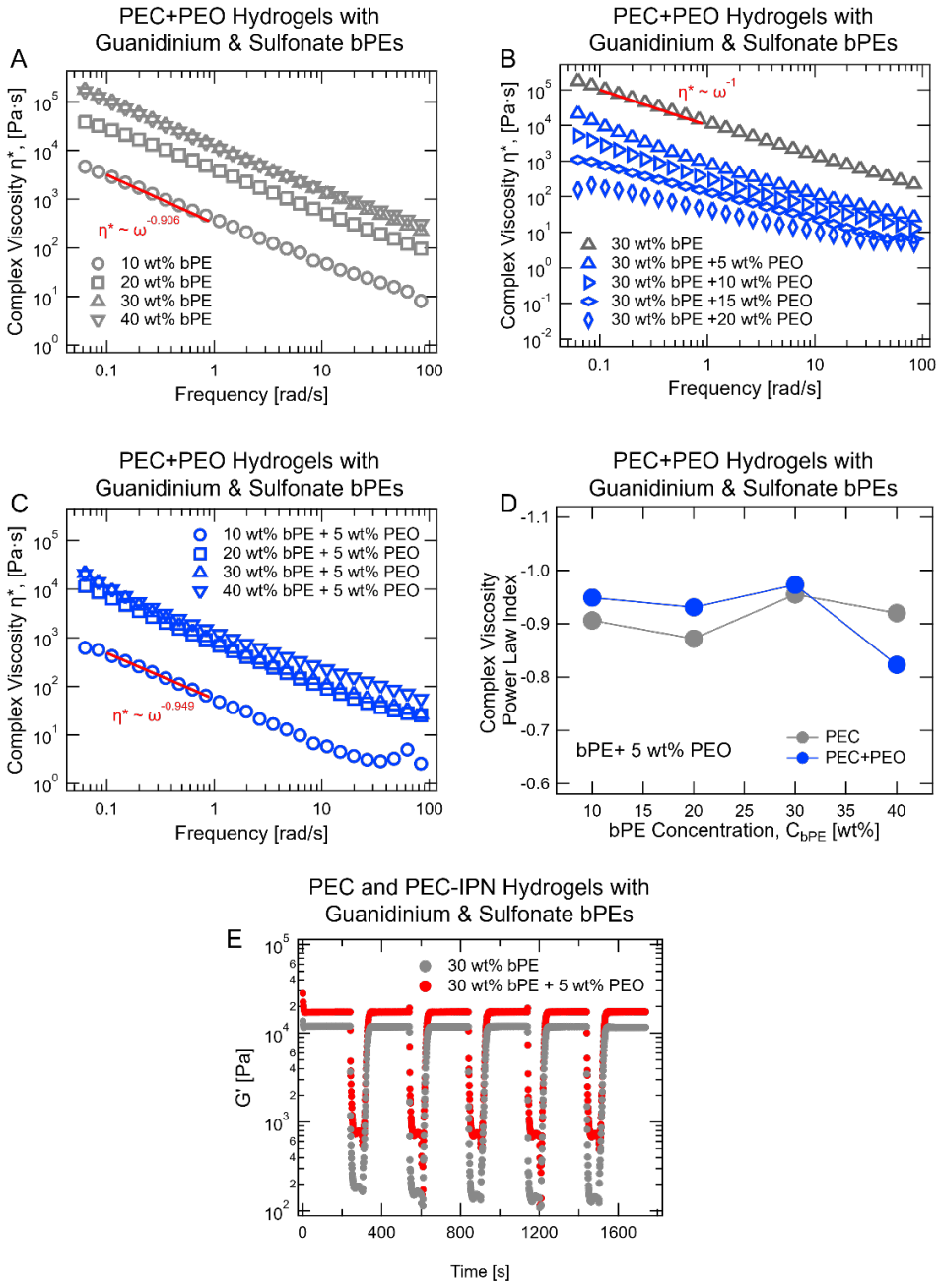

Figure S7. Representative complex viscosity and cyclic strain performance of PEC and PEC+PEO hydrogels comprising polyelectrolytes with guanidinium and sulfonate moieties. Complex viscosity (η^*) as a function of frequency (ω) for **(A)** PEC hydrogels with varying C_{bPE} from 10 wt% to 40 wt%, **(B)** PEC hydrogels (grey) with C_{bPE} (= 30 wt%) and PEC+PEO hydrogels with a constant C_{bPE} (= 30 wt%) and increasing C_{PEO} from 5 wt% to 20 wt%, and **(C)** PEC+PEO hydrogels with a fixed C_{PEO}(= 5 wt%) and increasing C_{bPE} from 10 wt% to 40 wt%. **(D)** Complex viscosity power law index (n, where $\eta^* \sim \omega^n$) for PEC and PEC+PEO hydrogels with C_{bPE} from 10 wt% to 40 wt%. PEC+PEO hydrogels contained a fixed C_{PEO} (= 5 wt%). **(E)** Cyclic strain performance of PEC hydrogels (grey) with C_{bPE} (=

30 wt%) and PEC-IPN hydrogels (red) with C_{bPE} (= 30 wt%) and C_{PEO} (= 5 wt%) PEO in the cyclic strains between 0.3% and 100%.

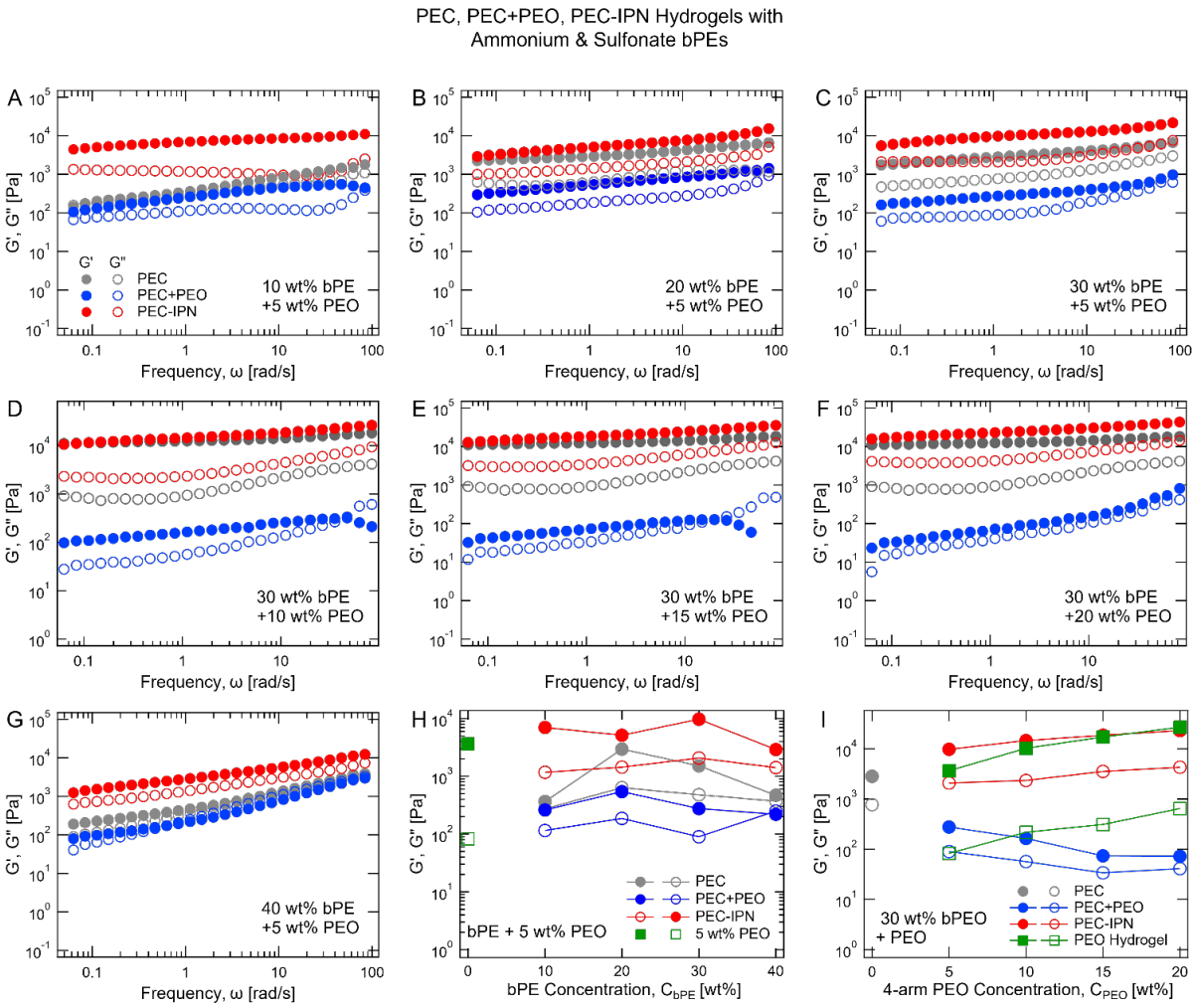

Figure S8. Modulations of shear strengths of PEC, PEO, PEC+PEO, and PEC-IPN hydrogels. (A-G) Storage (G') and loss (G'') moduli as a function of frequency (ω) for PEC hydrogels (grey), PEC+PEO hydrogels (blue), and PEC-IPN hydrogels (red) with varying C_{bPE} and C_{PEO}. **(H)** G' and G'' (at $\omega = 1.12$ rad/s) for PEO hydrogels (black) with C_{PEO}(= 5 wt%), PEC hydrogels (grey) with increasing C_{bPE} from 10 wt% to 40 wt%, PEC+PEO (blue) and PEC-IPN (red) hydrogels with a constant C_{PEO} (= 5 wt%) and increasing C_{bPE} from 10 wt% to 40 wt%. **(I)** G' and G'' (at $\omega = 1.12$ rad/s) for PEC hydrogels with C_{bPE} (= 30 wt%), PEO hydrogels with C_{PEO} from 5 wt% to 20 wt%, PEC+PEO hydrogels and PEC-IPN hydrogels with a constant C_{bPE} (= 30 wt%) and increasing C_{PEO} from 5 wt% to 20 wt%.

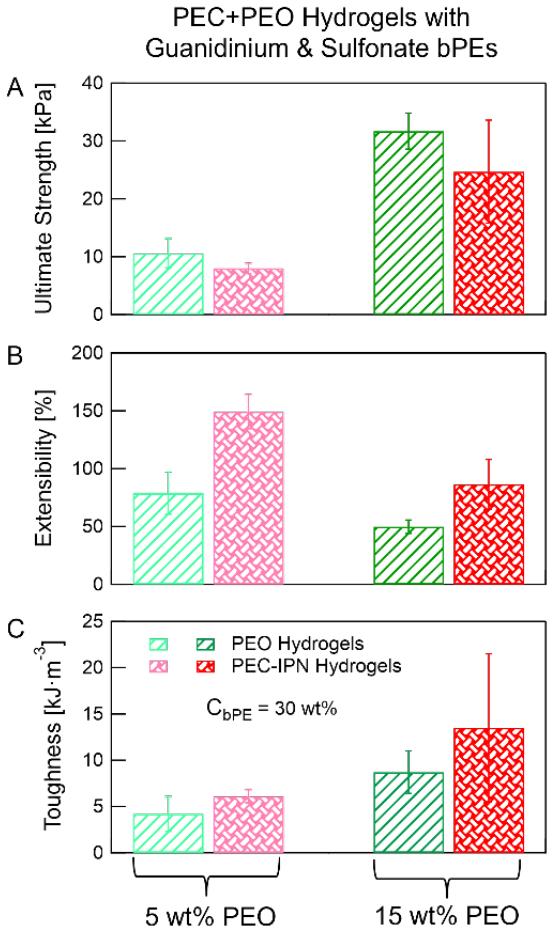

Figure S9. Tensile characterization for PEO hydrogels and PEC-IPN hydrogels comprising polyelectrolytes functionalized with guanidinium and sulfonate groups. (A) Ultimate strength, (B) extensibility, and (C) toughness. Data in (A–C) are averages obtained from measurements on three distinct samples.

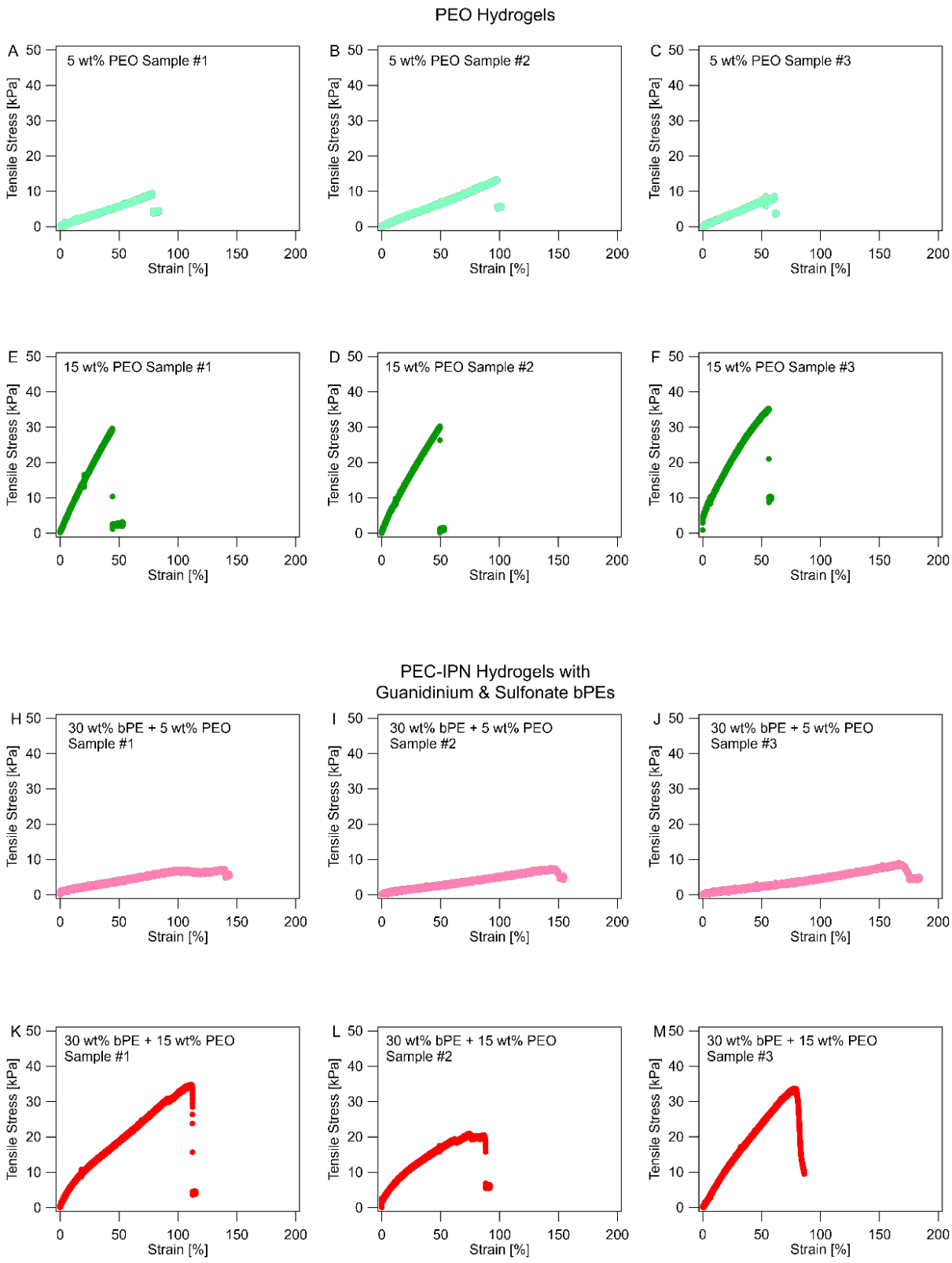

Figure S10. **Representative stress vs. strain curves for PEO and PEC-IPN hydrogels. (A-C)** PEO hydrogels with C_{PEO} (= 5 wt%), **(E-F)** PEO hydrogels with C_{PEO} (= 15 wt%), **(H-J)** PEC-IPN hydrogels with C_{bPE} (= 30 wt%) and C_{PEO} (= 5 wt%), **(K-M)** PEC-IPN hydrogels with C_{bPE} (= 30 wt%) and C_{PEO} (= 15 wt%).

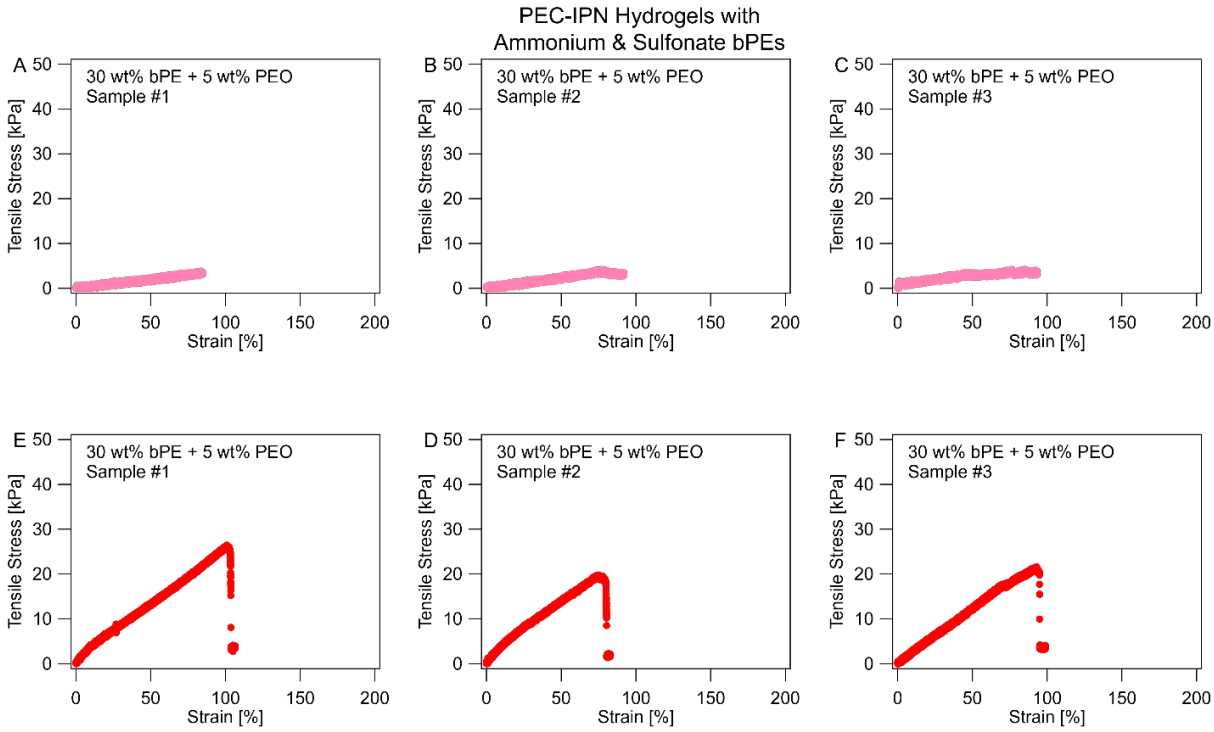

Figure S11. Representative Stress vs. strain curves for PEC-IPN hydrogels consisting of polyelectrolytes functionalized with ammonium and sulfonate groups. **(A-C)** PEC-IPN hydrogels with C_{bPE} (= 30 wt%) and C_{PEO} (= 5 wt%), **(E-F)** PEC-IPN hydrogels with C_{bPE} (= 30 wt%) and C_{PEO} (= 15 wt%).

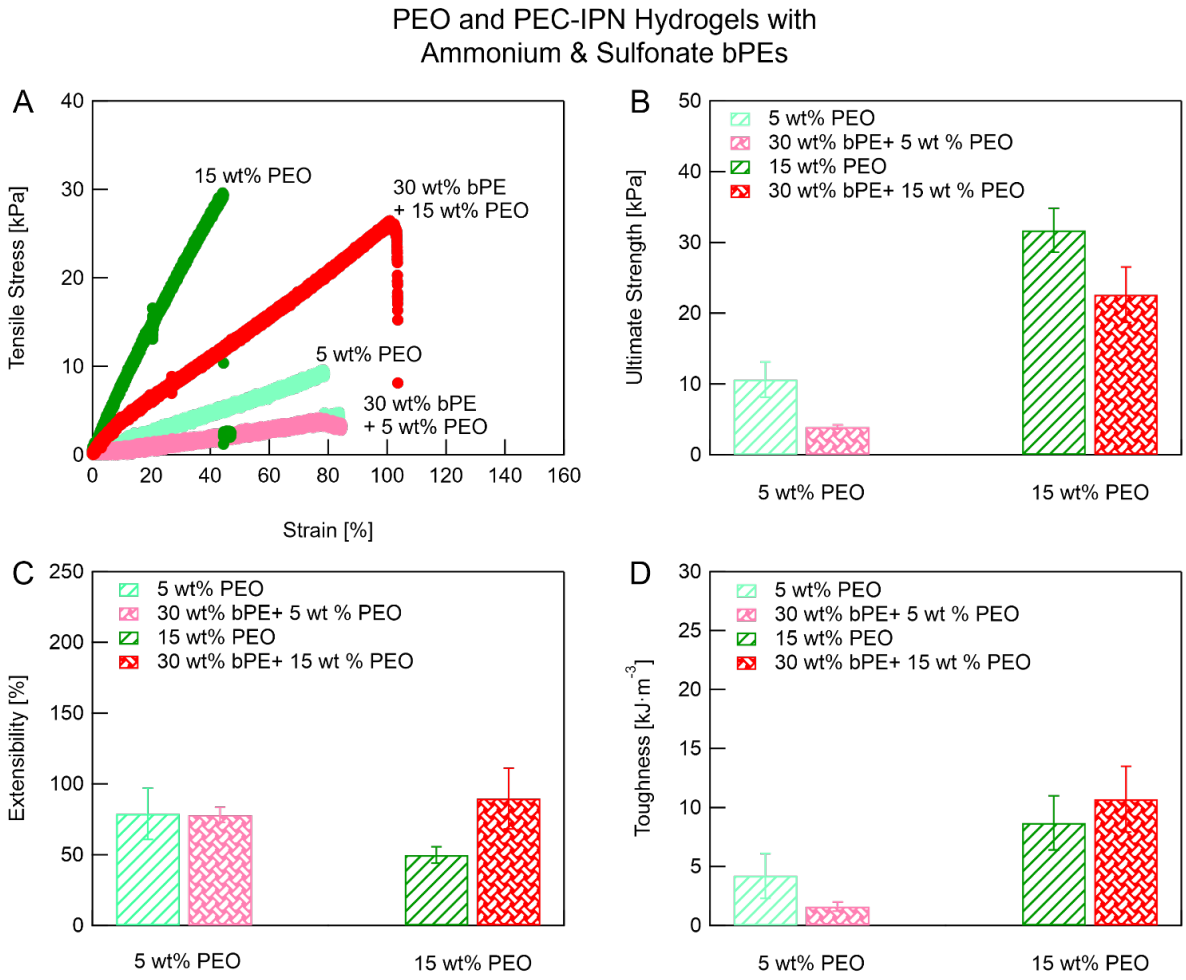

Figure S12. Tensile characterization for PEO hydrogels and PEC-IPN hydrogels comprising polyelectrolytes functionalized with ammonium and sulfonate groups. **(A)** Representative stress-strain curves, **(B)** ultimate stress, **(C)** extensibility, and **(E)** toughness for PEO and PEC-IPN hydrogels with C_{bPE} = 30 wt% and C_{PEO} = 5 wt% or 15 wt%. Data in (B–D) are averages obtained from measurements on three distinct samples.

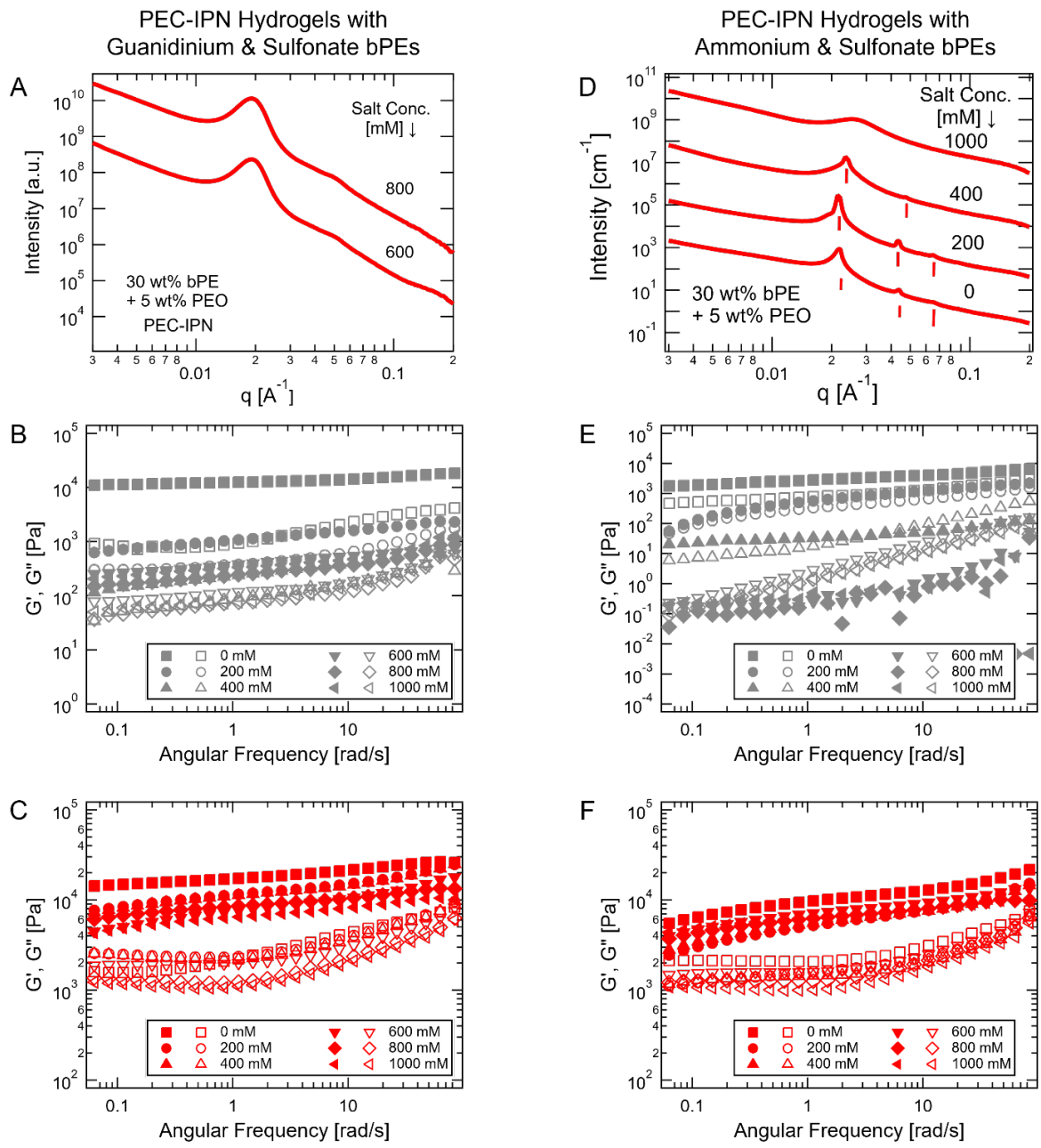

Figure S13. Evolution of microstructure and shear strength of PEC-IPN hydrogels in saline environments. (A) 1-D $I(q)$ versus wave vector q for PEC-IPN hydrogels (C_{bPE} = 30 wt% + C_{PEO} = 5 wt%) composed of block polyelectrolytes functionalized with guanidinium and sulfonate moieties and **(B-C)** the shear moduli (G' and G'') as a function of ω for PEC hydrogels (grey, C_{bPE} = 30 wt%) and PEC-IPN hydrogels (red, C_{bPE} = 30 wt% + C_{PEO} = 5 wt%) in saline environments with a variation of C_{salt}. **(D)**, **(E)**, and **(F)** show the data corresponding to (A), (B), and (C), respectively, for PEC-IPN hydrogels (C_{bPE} = 30 wt% + C_{PEO} = 5 wt%) and PEC hydrogels (C_{bPE} = 30 wt%) composed of block polyelectrolytes functionalized with ammonium and sulfonate moieties. In (A) and (D), the $I(q)$ spectra were shifted vertically for clarity.

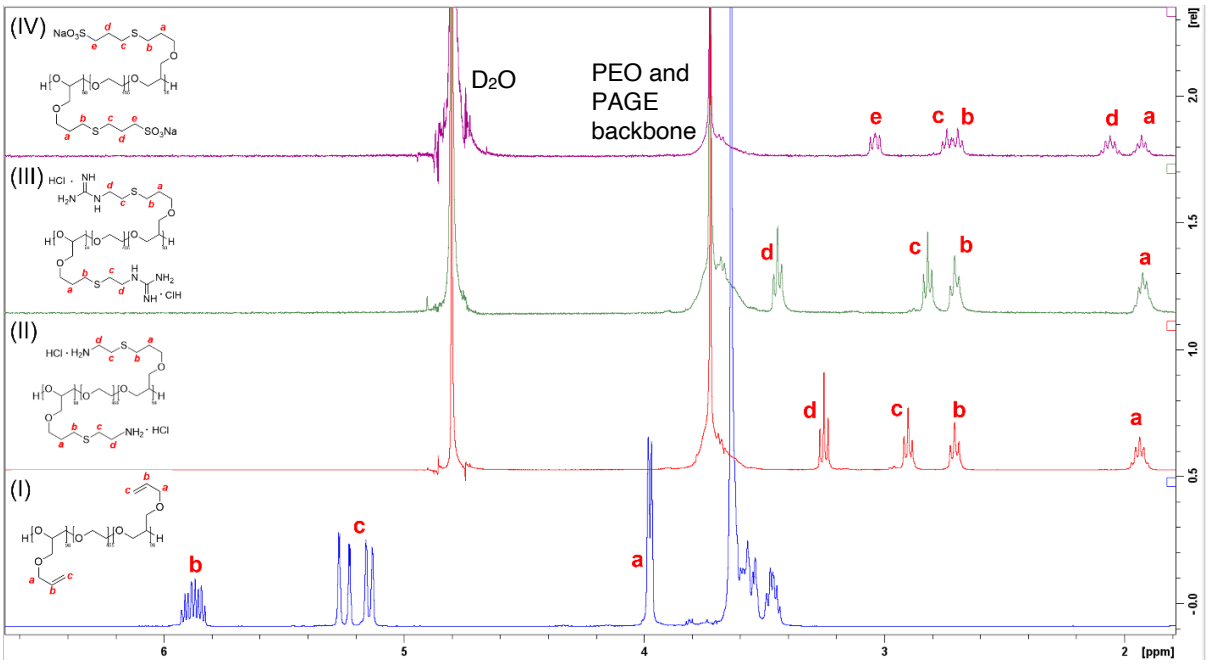

Figure S14. ^{1}H NMR spectra of **(I)** $PAGE_{98}$-PEO_{455}-$PAGE_{98}$, **(II)** ammonium-functionalized $PAGE_{98}$-PEO_{455}-$PAGE_{98}$, **(III)** guanidinium functionalized $PAGE_{98}$-PEO_{455}-$PAGE_{98}$, **(IV)** sulfonate-functionalized $PAGE_{98}$-PEO_{455}-$PAGE_{98}$.

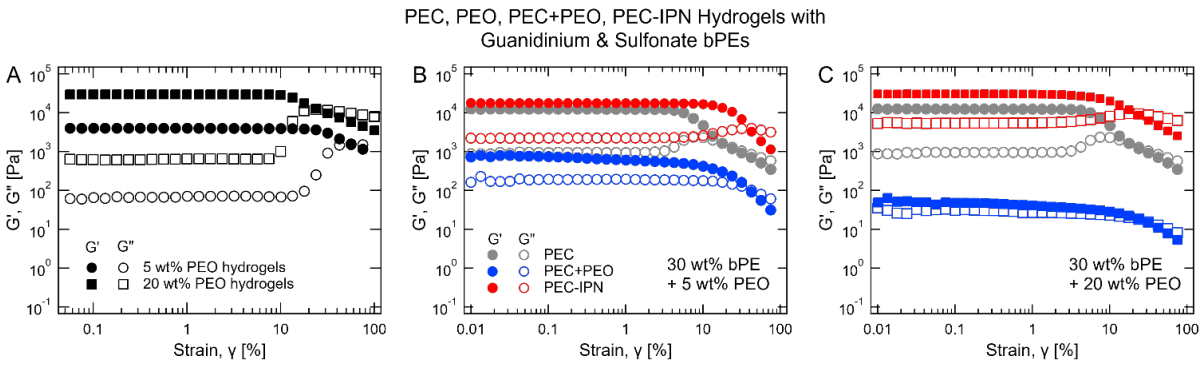

Figure S15. Representative amplitude sweeps showing the shear moduli (G' and G'') as a function of strain for PEO, PEC, PEC+PEO, and PEC-IPN hydrogels. (A) PEO hydrogels with C_{PEO} (= 5 wt% and 20 wt%), **(B)** PEC hydrogels (grey) with C_{bPE} (= 30 wt%), PEC+PEO hydrogels (blue) and PEC-IPN hydrogels (red) with C_{bPE} (= 30 wt%) and C_{PEO} (= 5 wt%), **(C)** PEC hydrogels (grey) with C_{bPE} (= 30 wt%), PEC+PEO hydrogels (blue) and PEC-IPN hydrogels (red) with C_{bPE} (= 30 wt%) and C_{PEO} (= 20 wt%).

Supplementary Tables

Table S1. Bragg peak locations and microstructure information for PEC+PEO and PEC-IPN hydrogels with a constant $C_{bPE} = 30$ wt% and varying C_{PEO}. The PEC+PEO and PEC-IPN hydrogels consisted of polyelectrolytes functionalized with guanidinium and sulfonate groups.

Hydrogel Description	q [Å^{-1}]	q/q^*	Expected q/q^*	Microstructure
PEC+PEO hydrogels with $C_{bPE} = 30$ wt% and $C_{PEO} = 15$ wt%	0.020	1.000	1.000	Lam
	0.038	1.928	2.000	
	0.057	2.888	3.000	
PEC-IPN hydrogels with $C_{bPE} = 30$ wt% and $C_{PEO} = 15$ wt%	0.021	1.000	1.000	Lam
	0.042	2.015	2.000	
	0.060	2.863	3.000	
PEC+PEO hydrogels with $C_{bPE} = 30$ wt% and $C_{PEO} = 20$ wt%	0.019	1.000	1.000	Lam
	0.036	1.914	2.000	
	0.054	2.889	3.000	
PEC-IPN hydrogels with $C_{bPE} = 30$ wt% and $C_{PEO} = 15$ wt%	0.021	1.000	1.000	Lam
	0.042	2.015	2.000	
	0.060	2.863	3.000	

Table S2. Bragg peak locations and microstructure information for PEC+PEO and PEC-IPN hydrogels with a constant C_{PEO} = 5 wt% and C_{bPE} = 30 wt% in the saline environments with different C_{salt}. The PEC+PEO and PEC-IPN hydrogels consisted of polyelectrolytes functionalized with ammonium and sulfonate groups.

Hydrogel Description	q [Å^{-1}]	q/q^*	Expected q/q^*	**Microstructure**
PEC+PEO hydrogels with C_{salt} = 0 mM	0.020	1.000	1.000	Lam
	0.041	2.064	2.000	
PEC-IPN hydrogels with C_{salt} = 0 mM	0.022	1.000	1.000	Lam
	0.044	1.993	2.000	
	0.064	2.885	3.000	
PEC+PEO hydrogels with C_{salt} = 200 mM	0.022	1.000	1.000	Lam
	0.044	1.993	2.000	
PEC-IPN hydrogels with C_{salt} = 200 mM	0.021	1.000	1.000	Lam
	0.044	2.052	2.000	
	0.065	3.017	3.000	
PEC+PEO hydrogels with C_{salt} = 400 mM	0.022	1.000	1.000	Lam
	0.044	1.993	2.000	
PEC-IPN hydrogels with C_{salt} = 400 mM	0.024	1.000	1.000	Lam
	0.047	2.000	2.000	

Table S3. Bragg peak locations and microstructure information for PEC+PEO and PEC-IPN hydrogels with a constant C_{PEO}= 5 wt% and varying C_{bPE}. The PEC+PEO and PEC-IPN hydrogels consisted of polyelectrolytes functionalized with ammonium and sulfonate groups.

Hydrogel Description	q [Å^{-1}]	q/q^*	Expected q/q^*	**Microstructure**
PEC hydrogels with $C_{bPE} = 30$ wt%	0.021	1.000	1.000	HCP Cylinder
	0.037	1.756	1.732	
	0.055	2.634	2.000	
PEC+PEO hydrogels with $C_{bPE} = 30$ wt% and $C_{PEO} = 5$ wt%	0.020	1.000	1.000	Lam
	0.041	2.064	2.000	
PEC-IPN hydrogels with $C_{bPE} = 30$ wt% and $C_{PEO} = 5$ wt%	0.022	1.000	1.000	Lam
	0.044	1.993	2.000	
PEC hydrogels with $C_{bPE} = 40$ wt%	0.022	1.000	1.000	Lam
	0.044	1.993	2.000	
	0.066	3.000	3.000	
PEC+PEO hydrogels with $C_{bPE} = 40$ wt% and $C_{PEO} = 5$ wt%	0.021	1.000	1.000	Lam
	0.043	2.000	2.000	
	0.064	2.970	3.000	
PEC-IPN hydrogels with $C_{bPE} = 40$ wt% and $C_{PEO} = 5$ wt%	0.022	1.000	1.000	Lam
	0.044	1.993	2.000	
	0.066	3.000	3.000	

Table S4. Bragg peak locations and microstructure information for PEC+PEO and PEC-IPN hydrogels with a constant $C_{bPE} = 30$ wt% and varying C_{PEO}. The PEC+PEO and PEC-IPN hydrogels consisted of polyelectrolytes functionalized with ammonium and sulfonate groups.

Hydrogel Description	q [Å^{-1}]	q/q^*	Expected q/q^*	Microstructure
PEC hydrogels with $C_{bPE} = 30$ wt%	0.021	1.000	1.000	HCP Cylinder
	0.037	1.756	1.732	
	0.055	2.634	2.000	
PEC+PEO hydrogels with $C_{bPE} = 30$ wt% and $C_{PEO} = 5$ wt%	0.020	1.000	1.000	Lam
	0.041	2.064	2.000	
PEC-IPN hydrogels with $C_{bPE} = 30$ wt% and $C_{PEO} = 5$ wt%	0.022	1.000	1.000	Lam
	0.044	1.993	2.000	
PEC+PEO hydrogels with $C_{bPE} = 30$ wt% and $C_{PEO} = 10$ wt%	0.020	1.000	1.000	Lam
	0.041	2.016	2.000	
	0.061	2.992	3.000	
PEC-IPN hydrogels with $C_{bPE} = 30$ wt% and $C_{PEO} = 10$ wt%	0.022	1.000	1.000	Lam
	0.043	1.942	2.000	
PEC+PEO hydrogels with $C_{bPE} = 30$ wt% and $C_{PEO} = 15$ wt%	0.020	1.000	1.000	Lam
	0.040	2.016	2.000	
	0.060	3.000	3.000	
PEC-IPN hydrogels with $C_{bPE} = 30$ wt% and $C_{PEO} = 15$ wt%	0.020	1.000	1.000	Lam
	0.039	1.968	2.000	
PEC+PEO hydrogels with $C_{bPE} = 30$ wt% and $C_{PEO} = 20$ wt%	0.021	1.000	1.000	Lam
	0.043	2.000	2.000	
	0.065	3.030	3.000	
PEC-IPN hydrogels with $C_{bPE} = 30$ wt% and $C_{PEO} = 20$ wt%	0.021	1.000	1.000	Lam
	0.043	2.000	2.000	

Supplementary Movies

Movie SM1. Movie depicting the injection, settling, and insolubility upon shaking of PEC hydrogels with $C_{bPE} = 10$ wt%. The PEC hydrogels consisted of bPEs functionalized with guanidinium and sulfonate groups.

Movie SM2. Movie depicting the injection, settling, and insolubility upon shaking of PEC+PEO hydrogels with $C_{bPE} = 10$ wt% and $C_{PEO} = 5$ wt%. The PEC+PEO hydrogels consisted of bPEs functionalized with guanidinium and sulfonate groups.

Movie SM3. Movie depicting the injection, settling, and solubility upon shaking of PEO precursor polymers with $C_{PEO} = 5$ wt%.